



University of  
Massachusetts  
Amherst

## Star Formation And Feedback In Smoothed Particle Hydrodynamic Simulations - I. Isolated Galaxies

Item Type	Article
Authors	Stinson, G;Seth, A;Katz, N;Wadsley, J;Governato, F;Quinn, T
DOI	<a href="https://doi.org/10.1111/j.1365-2966.2006.11097.x">10.1111/j.1365-2966.2006.11097.x</a>
Download date	2026-06-11 07:26:10
Link to Item	<a href="https://hdl.handle.net/20.500.14394/2989">https://hdl.handle.net/20.500.14394/2989</a>

# Star Formation and Feedback in Smoothed Particle Hydrodynamic Simulations—I. Isolated Galaxies

Greg Stinson<sup>1\*</sup>, Anil Seth<sup>1</sup>, Neal Katz<sup>2</sup>, James Wadsley<sup>3</sup>, Fabio Governato<sup>1,4</sup>, Tom Quinn<sup>1</sup>

<sup>1</sup>*Department of Astronomy, University of Washington, Box 351580, Seattle, WA 98195, USA*

<sup>2</sup>*Department of Astronomy, University of Massachusetts, Amherst, 01003, USA*

<sup>3</sup>*Department of Physics and Astronomy, McMaster University, Hamilton, Ontario L8S 4M1, Canada*

<sup>4</sup>*INAF, Osservatorio Astronomico di Brera, via Brera 29, 20121, Milano, Italy*

5 February 2008

## ABSTRACT

We present an analysis of star formation and feedback recipes appropriate for galactic smoothed particle hydrodynamics simulations. Using an isolated Milky Way-like galaxy, we constrain these recipes based on well-established observational results. Our star formation recipe is based on that of Katz (1992) with the additional inclusion of physically motivated supernova feedback recipes. We propose a new feedback recipe in which type II supernovae are modelled using an analytical treatment of blastwaves. With this feedback mechanism and a tuning of other star formation parameters, the star formation in our isolated Milky Way-like galaxy follows the slope and normalisation of the observed Schmidt law. In addition, we reproduce the low density cutoff and filamentary structure of star formation observed in disk galaxies. Our final recipe will enable better comparison of N-body simulations with observations.

**Key words:** star formation – supernova feedback – smoothed particle hydrodynamics.

## 1 INTRODUCTION

Meaningful comparisons between observations and simulations of galaxies require that simulations include gas and stars. While dark matter controls the global dynamics of galaxies, it cannot be directly observed. Gas and stars provide the photons that comprise observations. Unfortunately, for the foreseeable future, galaxy simulations will not be able to resolve individual stars, their individual explosions as supernovae, or the fine structure of gas clouds in the context of a galaxy. It is only possible to use a heuristic recipe to model the subresolution physics of star formation and the feedback effect of supernova explosions. Simulations that use the simplest methods of injecting supernova energy into the gas surrounding stars have proven ineffective at producing realistic star formation feedback (Katz 1992). The introduction of more clever sub resolution schemes for the distribution of supernova energy as a feedback on star formation (Thacker & Couchman (2001) and Springel & Hernquist (2003)) has resulted in more realistic disk galaxies.

The two methods currently employed to model gas physics in simulations are Eulerian grid codes and Lagrangian particle codes. Eulerian codes (e.g. Cen & Ostriker

(1993), Kravtsov (1999), and O’Shea et al. (2004)) track the movement of gas around a fixed grid of cells. The method that we describe in this paper involves a Lagrangian treatment of the gas called smoothed particle hydrodynamics (SPH) (Monaghan 1992). Resolution is achieved naturally as particles concentrate in dense regions of interest. To solve the equations of hydrodynamics, physical quantities are determined using spline kernel interpolation of neighbouring particles.

Various methods have been employed to convert these smoothed gas particles into stars. Evidence of the improvement in the resolution of simulations is that early work (Cen & Ostriker 1993) changed dense gas into “galaxy particles”. More recent codes (Yepes et al. 1997; Hultman & Pharasyn 1999; Springel & Hernquist 2003) choose to package stars along with hot and cold gas into multiphase particles corresponding to the cold/warm and hot phases of the ISM reported in McKee & Ostriker (1977). Physical properties like temperature and density of the multiphase particles are assumed to be the average of the different components of each particle. In one version of multiphase particles (‘explicit’), Springel & Hernquist (2003) allow gas particles to host stellar mass, spawning stars once the stellar component of the multiphase particle exceeds a minimum star particle mass.

Using the SPH code GASOLINE (Wadsley et al. 2004),

\* E-mail: stinson@astro.washington.edu

we choose to follow a different method that is outlined in Katz (1992), one that uses a stochastic formulation for star formation (see also Kawata & Gibson (2003), the ‘ordinary’ star formation in Springel & Hernquist (2003), and Okamoto et al. (2005)). This allows stars to form immediately and gas particles to maintain their own, unique character and temperature, hot, cold or warm. As supernovae are the direct result of star formation, we use them as the feedback that limits star formation. The coarse mass and spatial resolution of current simulations limits models to heuristic descriptions of this phenomenon. The insufficient resolution and lack of multiple gas phases also means that the  $10^{51}$  ergs of energy that a supernova generates, if deposited as thermal energy, would be dissipated through radiative cooling processes before that thermal energy has any effect on the gas surrounding the supernova explosion (e.g. Katz et al. 1996; Brook et al. 2004).

Two methods have been employed to use that energy in other ways. Navarro & White (1993) describe a kinematic feedback mechanism that uses the supernova energy to provide an outwards velocity kick to all of the gas particles surrounding a star particle in which a supernova (or more commonly a large group of supernova) has exploded. Springel & Hernquist (2003) use this idea to individually kick their multiphase particles in some direction, either randomly or perpendicular to their angular momentum vector, after a supernova has exploded. Even in such kinematic approaches the feedback does not have a very strong effect, i.e. it is not efficient in driving winds from small galaxies, unless the hydrodynamic forces are temporarily turned off as in Springel & Hernquist (2003).

An alternative to these kinematic examples is to more effectively mimic the transfer of the kinetic energy of supernova shockwaves to thermal energy in the interstellar medium (ISM). Yepes et al. (1997) and Hultman & Pharasyn (1999) both utilise multiphase components and convert some multiple of the mass in stars undergoing type SNII explosions from a cold gas phase to a separate hot gas phase. Alternatively, Pearce et al. (1999) assigned gas particles to one of two phases in SPH simulations. The phase separation can limit the loss of thermal energy deposited from supernova feedback (Marri & White 2003). In contrast, Gerritsen (1997) does not explicitly use multiphase particles but turns off the radiative cooling of the gas particles immediately surrounding a star particle in which SNII have recently exploded. Thacker & Couchman (2000); Bottema (2003) examined how the Gerritsen (1997) scheme works in an isolated Milky Way galaxy. Thacker & Couchman (2001); Sommer-Larsen et al. (2003); Governato et al. (2006) used this recipe in cosmological simulations of forming galaxies. Pelupessy et al. (2004) explored how this recipe worked in the environment of isolated disk dwarf galaxies. Brook et al. (2004) showed that the adiabatic feedback method produces more realistic feedback in simulations of isolated collapsing halos.

We extend the exploration of the recipe started in Thacker & Couchman (2000) for the case of an isolated Milky Way galaxy here with the goal of further refining the star formation and feedback algorithm. This paper specifically focuses on the star formation recipe first described in Katz (1992) paired with feedback that for a time cools

only adiabatically to prevent immediate radiative losses as described in Thacker & Couchman (2000). Because of this focus, we are able to optimise the recipe, present a full parameter study and include investigations of specific issues like the resolution dependence of star formation and feedback.

§2 describes the details of the recipe that we test to convert gas into stars and §3 describes our feedback schemes. §4 presents the tunable parameters that affect star formation in our isolated model Milky Way (IMMW). §5 presents the results of varying the criteria and parameters and determines which choices work best at reproducing observations for the IMMW. §6 discusses the relevance and plausibility of our recipe and possible future improvements. We present our final star formation and feedback recipe and conclude in §7.

## 2 STAR FORMATION

Our star formation algorithm is similar to the one proposed in Katz (1992) and extended in Katz et al. (1996, hereafter KWH). First, we apply criteria to determine which gas particles are eligible to form stars. We then determine which gas particles actually form stars probabilistically such that on average we reproduce a star formation rate formula similar to a Schmidt law (Schmidt 1959). Those gas particles that actually form stars spawn a new star particle of a pre-determined mass, reducing their own mass accordingly. The new star particle is created with the same velocity, position, and metallicity as its parent gas particle. Star particles can add energy, mass and metals back to gas particles through feedback processes including type II and Ia supernova and stellar winds.

### 2.1 Criteria

The recipe proposed in Katz (1992) and KWH starts with an examination of every SPH gas particle in the simulation. The gas particle must satisfy 4 criteria before it is eligible for star formation:

- Is the particle denser than  $n_{\min} = 0.1 \text{ cm}^{-3}$ ?
- Is the particle in an overdense region?
- Is the particle part of a converging flow?
- Is the particle Jeans unstable ( $\frac{h_z}{c_i} > \frac{1}{\sqrt{4\pi G \rho_i}}$ )?

The density and overdensity criteria simply check that particles fall above the limits set for the simulation. We choose the overdensity limit to be  $55 \rho/\bar{\rho}$ , which limits star formation to virialised regions at early times in the Universe when the physical density everywhere is high and plays no role in simulations of isolated galaxies. It is a simple matter to adjust these limits to match observed galaxy properties. In this paper we use  $n$  to represent the number density ( $\text{cm}^{-3}$ ) and  $\rho$  to represent the mass density ( $\text{g cm}^{-3}$ ). For gas particles  $n\mu m_H = \rho$ , where  $\mu$  is the mean molecular weight and  $m_H$  is the mass of a Hydrogen atom.

Katz (1992) made the reasonable assumption that the gas forming a star should be in a collapsing region and so required that the gas particles be part of a converging flow. In our implementation of SPH every particle is assigned a

smoothing length,  $h$ , such that there are a fixed number of particles (neighbours),  $N_{\text{smooth}}$ , within twice that length. We usually choose  $N_{\text{smooth}}$  to be 32. Physical quantities are estimated using spline kernel interpolation. For example, the mass density,  $\rho$ , for particle  $i$  is given by

$$\rho_i = \sum_{j=1}^N m_j W(|\mathbf{r}_i - \mathbf{r}_j|, h_i, h_j) \quad (1)$$

where  $m$  is the particle mass,  $N$  is the number of gas particles, and  $W$  is the smoothing kernel, which we choose to have compact support, i.e. it goes to zero beyond  $2h$  so the sum is really only over  $N_{\text{smooth}}$  (Monaghan 1992; Hernquist & Katz 1989). The divergence of the velocity field,  $\nabla \cdot \mathbf{v}$  at the position of gas particle  $i$  is given by

$$\nabla \cdot \mathbf{v} = \frac{1}{\rho_i} \sum_{j=1}^N m_j (\mathbf{v}_j - \mathbf{v}_i) \cdot \nabla_i W(|\mathbf{r}_i - \mathbf{r}_j|, h_i, h_j) \quad (2)$$

where  $\mathbf{v}$  is the velocity. When  $\nabla \cdot \mathbf{v}$  is negative, the criterion is satisfied, it is assumed that the gas particle is part of a collapsing flow, and the gas particle can form stars.

The Jeans Criterion is a test of whether or not a gas cloud can provide pressure support against gravitational collapse. If a sound wave cannot travel across the cloud in the time it would take the cloud to gravitationally free fall to the centre, then the cloud will collapse. Katz (1992) proposed that such a criterion should take the form:

$$\frac{h_i}{c_i} > \frac{1}{\sqrt{4\pi G \rho_i}} \quad (3)$$

where  $c_i$  is the sound speed of the gas particle in question and  $G$  is the gravitational constant. This tests if the temperature and pressure of one particle inside its smoothing sphere would be able to support the whole sphere against gravitational collapse. Katz (1992) only applies this criterion when the region is not affected by gravitational softening, but Okamoto et al. (2003) notes that the Jeans Criterion formulated in this way is similar to the Bate & Burkert (1997) resolution limit for artificial fragmentation. In §2.1, it is shown that this formulation of the Jeans criterion introduces a resolution dependence and hence we will eliminate it from our final formulation.

## 2.2 Stochastic Star Formation

Ideally, stars should form whenever specific criteria like those described above are met (see also Li et al. (2005a) or Michel-Dansac & Wozniak (2004)). However, since our simulations of galaxies have limited resolution we can only capture the global behaviour of star formation, and we use a probabilistic approach.

Katz (1992) bases the number of stars that form on the theoretical star formation rates of Larson (1969) and Silk (1987), who both proposed that  $\rho_{\text{SFR}} \sim \rho_{\text{gas}}^{3/2}$ , where  $\rho$  is the volume density. These formulations make use of the fact that the dynamical time,  $t_{\text{dyn}} \sim \rho^{-1/2}$ . However, to form stars gas must also cool so Katz (1992) chose the star formation timescale,  $t_{\text{form}}$ , to be the maximum of the dynamical time and the cooling time. If the gas was already cool enough to form stars, i.e.  $T < T_{\text{max}}$ , then  $t_{\text{dyn}}$  was used. Katz (1992) took  $T_{\text{max}} = 30,000\text{K}$ , which was appropriate given his cooling function. So one can write the star formation rate as

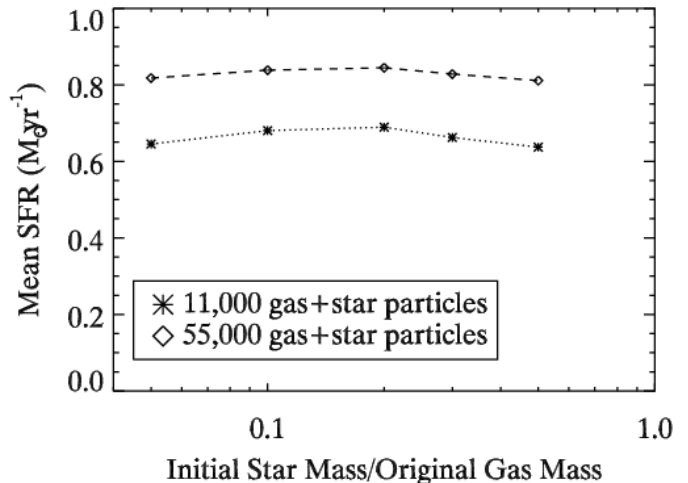


**Figure 1.** The mean star formation rate (SFR) as a function of the star particle mass in units of the original gas particle mass. The SFR shows little dependence on the initial star particle mass. These results are for our fiducial values of parameters and criteria on the isolated model Milky Way (IMMW) described in §4.

$$\frac{d\rho_*}{dt} = c^* \frac{\rho_{\text{gas}}}{t_{\text{form}}} \quad (4)$$

where we have introduced a constant efficiency factor  $c^*$  that will enable us to adjust the star formation rate to match observations. We will choose to set  $t_{\text{form}} = t_{\text{dyn}}$  at all times and instead will introduce another star formation criterion that  $T < T_{\text{max}}$ .

Because of the dependence on density, it is possible to create a stochastic recipe for when and where stars should form. If one takes the probability that a star will form as

$$p = \frac{m_{\text{gas}}}{m_{\text{star}}} \left( 1 - e^{-c^* \Delta t / t_{\text{form}}} \right) \quad (5)$$

where  $m_{\text{gas}}$  is the mass of the gas particle and  $m_{\text{star}}$  is the mass of the potentially spawned star particle then on average one recovers Equation (4).

In this formulation there is a greater probability of a star forming in denser areas. For each star formation eligible gas particle a random number,  $r$ , is drawn between zero and one and if  $r < p$  a new star particle is created. Katz (1992) assumed that the star particle mass was always a constant fraction of the parent gas particle mass, i.e.  $m_{\text{star}}/m_{\text{gas}} = \epsilon^*$ . In that case,  $\epsilon^{*-1}$  replaces  $m_{\text{gas}}/m_{\text{star}}$  in Equation (5).  $\epsilon^*$  can be absorbed into the definition of  $c^*$ , for the relevant case where  $\Delta t/t_{\text{form}}$  is small, and hence does not appear in Equation (5) of Katz (1992). Therefore, to compare with Katz (1992),  $c^*$ 's here should be multiplied by  $\epsilon^*$ . Here we are interested in making the new star particle have a constant mass to remove the large variation in star particle mass that can occur as stars form at different times during the simulation. Using Equation (5) and assuming a constant stellar particle mass we can recover the same global star formation rate, almost independent of that mass, as shown in Figure 1. A smaller star particle mass gives us better resolution for the stellar component at the cost of greater computational expense and we choose a value of  $0.2 \times$  the initial gas particle mass as a compromise.

Codes that use multiphase gas particles for star formation, e.g. Springel & Hernquist (2003) ‘explicit’ star formation, more finely time sample star formation since a specific amount of gas is converted into stars during every gas particle timestep and new star particles are only spawned periodically. However, this approach has an inherent problem. When feedback occurs, stars that are still tied to their parent gas particles can get hydrodynamically accelerated and possibly even be ejected from the galaxy, which is not physical.

One problem that could arise when using a stochastic approach for star formation is that particularly dense regions might not experience the vigorous star formation that is observed in starburst galaxies (Telesco 1988; Chapman et al. 2003) if the mass of all star particles is fixed. A possible solution to this problem is to make the mass of the star particle that forms dependent on properties of the gas particle. For instance, Elmegreen & Efremov (1997) provide a formula using the density and the pressure of gas to determine what fraction of the gas will form stars. Initial tests using this formula suggest that our resolution is too coarse for this recipe to yield useful results. However, for our fiducial parameters, a star particle mass 0.2 times the initial gas particle mass and a star formation interval,  $\Delta t$ , of 1 Myr, this problem would only arise if gas consumption times become less than 5 Myr, a situation that is rarely, if ever, observed.

### 3 FEEDBACK

Katz (1992) and KWH add mass and energy feedback from type II supernova. The energy is added gradually with an exponential decay rate of 20 Myr. It is added at the location of the parent gas particle and is smoothed using the SPH smoothing kernel. Since this thermal energy is typically added to very dense gas, it is quickly radiated away and has little effect on the evolution of the galaxy. We describe a stronger and perhaps more realistic method for including type II supernovae (SNII) feedback (Gerritsen 1997), which we implement here. In addition we now also include feedback from type Ia supernovae and stellar winds from planetary nebulae and allow the metals produced in our stars to be distributed. Their implementation is described towards the end of this section.

#### 3.1 Type II Supernovae (SNII)

SNII play a dominant role in regulating star formation in our simulations because of their ability to heat large volumes of the interstellar medium near the site of star formation and consequently prevent more gas from collapsing (Silk 2003). Because the blastwave shocks of SNII convert the kinetic energy of ejecta into thermal energy on scales smaller than our simulations resolve, feedback in our simulations is purely thermal.

The number of supernovae produced by a star particle depends on the initial mass function of the stars that form. We use the three piece power law fit of the IMF defined in Miller & Scalo (1979), where  $\alpha = -0.4$  for stars with masses between 0.1 and 1  $M_{\odot}$ ;  $\alpha = -1.5$  for stars with masses between 1 and 10  $M_{\odot}$ ;  $\alpha = -2.3$  for stars with masses greater than 10  $M_{\odot}$ . Our IMF starts at 0.1  $M_{\odot}$  because Reid et al.

(2002) report that the stellar luminosity function appears to turn over at a luminosity corresponding to that mass, so that stars with a mass  $< 0.1 M_{\odot}$  do not make a large contribution to the total stellar mass.

The time when a star explodes as a supernova depends on its lifetime. We use the Raiteri et al. (1996) parameterisation of the Padova group’s (Alongi et al. 1993; Bressan et al. 1993; Bertelli et al. 1994) stellar lifetime calculations for stars of varying metallicities. In this parameterisation, since more massive stars have shorter lifetimes than small mass stars, it is possible to determine the maximum and minimum stellar mass that will explode during a given timestep and, therefore, integrating over the initial mass function provides the total mass and number of stars that will explode. Like the Raiteri et al. (1996) recipe, we only allow stars between 8 and 40  $M_{\odot}$  to explode as SNII; stars more massive than this are assumed to either collapse into black holes or explode as type Ib supernovae. Regardless, few stars form with masses greater than 40  $M_{\odot}$ , so the impact on the feedback is minimal. The use of stellar lifetimes is an improvement on previous SN feedback recipes that bled the supernova energy out gradually as some type of exponential function after a star particle formed (Cen & Ostriker 1993, KWH). Thus, many implementations of feedback choose to use them now (Lia et al. 2002; Kawata & Gibson 2003; Okamoto et al. 2003; Scannapieco et al. 2005).

We multiply the number of SNII that explode by the energy ejected into the ISM,  $E_{\text{SN}}$ , a fixed fraction of the canonical  $10^{51}$  ergs produced by a supernovae, and distribute that energy to the surrounding gas particles. The energy is spread out, weighted by the mass of the gas particle that receives it, using the SPH smoothing kernel. Unlike in Katz (1992) and KWH, however, the feedback is centred on the current position of the star particle and not on the parent gas particle. Therefore, the feedback energy received by a neighbouring gas particle  $i$  for a total feedback energy of  $\Delta E_{\text{SN}}$  is just

$$\Delta E_{\text{SN},i} = \frac{m_i W(|\mathbf{r}_i - \mathbf{r}_s|, h_s) \Delta E_{\text{SN}}}{\sum_{j=1}^N m_j W(|\mathbf{r}_j - \mathbf{r}_s|, h_s)} \quad (6)$$

where  $h_s$  is the distance from the star particle to its 32nd closest neighbouring gas particle. We explore how star formation depends on  $E_{\text{SN}}$  in §5. When  $E_{\text{SN}} = 10^{50}$  ergs,  $7.65 \times 10^{47}$  ergs of energy are deposited into the surrounding gas for every one  $M_{\odot}$  of stars formed. Metal production follows Raiteri et al. (1996), where the ejected oxygen and iron mass are estimated using a power law based on the mass that Raiteri et al. (1996) estimated from Woosley & Weaver (1995). We integrate this power law between the minimum and maximum mass stars that explode during a given timestep to determine the mass of oxygen and iron ejected into the ISM. The metals and the mass returned to the gas particles by the type II supernova are distributed in a way similar to Equation (6).

Unfortunately, the distributed feedback energy will have little impact on our simulated galaxies owing to our finite resolution and inability to resolve the complex multiphase interstellar medium properly. Since the supernovae explode in regions of high average density, the gas can radiate away the energy in much less time than a typical timestep. To make the feedback more realistic we tried two different approaches (see §3.1.1 and §3.1.2) to mimic blastwaves, which

should take hundreds of thousands of years to cool. In both approaches we disable the radiative cooling in a number of the nearest gas particles.

Disabling the radiative cooling in the surrounding gas particles allows us to model two different aspects of the feedback phenomenon. First, the gas particles immediately surrounding new stars have their cooling disabled, and with the added energy from the supernovae, will likely become hotter than the maximum temperature,  $T_{\max}$ , allowed for forming stars. In this way, feedback inhibits further star formation in dense regions much like supernovae generate turbulence in molecular clouds, which provides global stability against further collapse of the entire molecular cloud. Secondly, the increased temperature of the gas particle models the high pressure of a blastwave, which plays a key role in shaping the interstellar medium, allowing the surrounding gas to naturally flow outwards.

In our initial scheme, we determine the number of gas particles that have their cooling disabled by multiplying the SNII mass by a mass loading factor,  $\beta$ , and shutoff the cooling for a constant time,  $\tau_{\text{CSO}}$ . Our other scheme requires fewer parameters because it depends on the analytic treatment of blastwaves described in McKee & Ostriker (1977).

Both schemes allow gas particles to receive energy from multiple supernovae explosions in a similar fashion. Every timestep, each gas particle has its cooling shutoff time,  $\tau_{\text{CSO}}$  calculated from the total supernova energy received. For subsequent supernova,  $\tau_{\text{CSO}}$  is recalculated and extended when necessary.

### 3.1.1 Supernova Mass Factor ( $\beta$ ) Recipe

We derive the mass loading factor concept from multi-phase recipes like Yepes et al. (1997) and Hultman & Pharasyn (1999). We calculate the exact number of gas particles where we turn off the radiative cooling in the following manner. For gas particles surrounding a star particle, radiative cooling is disabled for gas particles within a sphere of mass  $\beta M_{\text{SNII}}$ . For a gas particle  $i$ , if

$$\beta M_{\text{SNII}} > \frac{4\pi(|\mathbf{r}_i - \mathbf{r}_s|)^3}{3} \rho_{\text{ave}} \quad (7)$$

where  $M_{\text{SNII}}$  is the mass of stars that go supernovae during a given timestep,  $(|\mathbf{r}_i - \mathbf{r}_s|)$  is the distance from the star to the gas particle in question, and  $\rho_{\text{ave}}$  is given by

$$\rho_{\text{ave}} = \sum_{j=1}^N m_j W(|\mathbf{r}_s - \mathbf{r}_i|, h_s). \quad (8)$$

The maximum number of particles for which we can disable the cooling is  $N_{\text{smooth}}$ , which is 32 in our simulations.

In our initial recipe, cooling is disabled for a fixed amount of time,  $\tau_{\text{CSO}}$ . We started with  $\tau_{\text{CSO}} = 30$  Myr based on the work of Gerritsen (1997) and Thacker & Couchman (2000) who suggest that  $8 M_{\odot}$  stars have a lifetime of 30 Myr (although using the Padova tracks it would be closer to 38 Myr). Thus, after 30 Myr, feedback produced in a star forming region should be finished. We explore the effects of varying  $\tau_{\text{CSO}}$  in §5.2.2.

### 3.1.2 Blastwave Recipe

Exploration of the  $\beta$  parameter motivated us to introduce an explicit blastwave solution based on Chevalier (1974) and McKee & Ostriker (1977). This solution reduces the number of tunable parameters by providing both the maximum radius to which the blastwave explosion will reach and the time that the blastwave will keep the gas hot. The maximum radius of a supernova blastwave in the Chevalier (1974) simulations was

$$R_E = 10^{1.74} E_{51}^{0.32} n_0^{-0.16} \tilde{P}_{04}^{-0.20} \text{pc} \quad (9)$$

where  $E_{\text{SN}} = E_{51} 10^{51}$  ergs,  $n_0$  is the ambient Hydrogen density,  $\tilde{P}_{04} = 10^{-4} P_0 k^{-1}$  where  $P_0$  is the ambient pressure and  $k$  is the Boltzmann constant. Both  $n_0$  and  $P_0$  are calculated using the SPH kernel for the gas particles surrounding the star. We temporarily turn off the radiative cooling for all gas particles within  $R_E$ . However, there is an artificial maximum of 32 particles that can have their cooling disabled. Figure 18 shows how many of these particles there are typically.

The simulations also provide a timescale for the time that a gas particle does not radiatively cool. Naively, one might think that this timescale should be the length of the Sedov phase of a supernova explosion. During this phase, energy is conserved in the supernova remnant because it is not able to effectively radiate. However, the Sedov phase only lasts for tens of thousands of years (Padmanabhan 2001). Our simulations cannot resolve this timescale and the feedback would be ineffective even if our simulations produce clusters of supernova. Also, McKee & Ostriker (1977) suggest that a hot, low density shell survives well after the Sedov phase.

Following the Sedov phase, blastwaves enter the snowplow phase. During the snowplow phase, momentum is conserved as the blastwave expands because the gas has cooled enough to radiate more efficiently. McKee & Ostriker (1977) present the end of the snowplow phase when a supernova remnant first reaches its maximum extent:

$$t_E = 10^{5.92} E_{51}^{0.31} n_0^{0.27} \tilde{P}_{04}^{-0.64} \text{yr} \quad (10)$$

The supernova remnant continues to cool radiatively even after it stops expanding. McKee & Ostriker (1977) report that the time that the hot, low density shell will survive is

$$t_{\max} = 10^{6.85} E_{51}^{0.32} n_0^{0.34} \tilde{P}_{04}^{-0.70} \text{yr} \quad (11)$$

Either of these timescales may be appropriate for the length of time to disable cooling and we report on how using either  $t_E$  or  $t_{\max}$  affects star formation in §5.3.1.

Even in the case where a supernova has exploded in a previous timestep, we currently use the previous equations as described. We are investigating the possible interactions of multiple supernovae remnants. As an initial assumption, we suppose that all of the supernovae exploding during a given timestep combine their energy to generate the blastwave.

### 3.1.3 Small SN Smoothing

Since we only disable cooling for a fraction of the particles within the smoothing radius, it is only those particles that maintain the high temperature generated from the supernova. Thus, all the energy that gets distributed beyond the

blast radius is quickly radiated away, which is still unphysical. To address this problem, we introduce another variant of the blastwave approach where we restrict the distribution of energy from the supernova only to those particles within the blast radius using a kernel function limited to just the particles within the blast radius. Initial trials only distributed metals and mass inside the blast radius like the energy. However, as we have yet to implement diffusion of metals between gas particles, the supernova explosion represents the only time when metals can be widely distributed. Distributing metals only inside the blast radius lead to spurious metal distributions. Thus, we reverted to distributing the metals and mass across the entire smoothing sphere.

It sometimes occurs that no particle is within the blast radius. In this case, we deposit the energy, metals, and mass to the nearest gas particle. Ejecta are distributed in this manner for both SNII and SNIa, but for SNIa, the cooling is not disabled. If there are no supernova ejecta, the wind feedback is distributed across all 32 nearest neighbours with the standard smoothing radius.

Such an approach might be a cause for concern since Benz & Thielemann (1990) have found that depositing energy into a single gas particle in a SPH simulation can lead to overcooling and a violation of energy conservation owing to the large energy gradient introduced. However, Springel & Hernquist (2002) show that this is not a problem if one uses the asymmetric form of the thermal energy equation, as we do in GASOLINE.

### 3.2 Type Ia Supernovae (SN Ia)

SNIa are also significant sources of metals and are thought to occur in binary systems. The method we use to determine how many SNIa explode is again described in detail in Raiteri et al. (1996). The minimum mass of a binary system is  $3 M_{\odot}$  and the maximum mass is  $16 M_{\odot}$  (two  $8 M_{\odot}$  stars). Using the binary fractions from Raiteri et al. (1996) makes the number of SNIa 10-20 % of the total supernovae in our Isolated Model Milky Way simulations, as observed by van den Bergh & McClure (1994) in spiral galaxies.

Usually we distribute the SNIa energy using the smoothing kernel amongst the  $N_{\text{smooth}}$  nearest neighbouring gas particles. However, for those star particles that also distribute SNII energy within the blast radius, the SNIa energy is also only distributed within the blast radius.

Radiative cooling is not disabled as a result of SN Ia because SN Ia occur much after the stars initially form. During this time, stars would dynamically spread out of their initial associations and subsequent SNIa would not be a collective phenomenon, like SNII, and hence would not lead to large blastwaves. Since stars in our simulations consist of indivisible particles, the SNIa stars cannot drift apart as they should, would act collectively and produce too large an effect if we turned off the cooling. Our early simulations indicated the inclusion of SNIa produced too large of a feedback effect.

Like energy, mass and metals are smoothed across all  $N_{\text{smooth}}$  nearest neighbour particles. All SNIa are assumed to eject the same mass ( $1.4 M_{\odot}$ ) and the same amount of iron ( $0.63 M_{\odot}$ ) and oxygen ( $0.13 M_{\odot}$ ) based on the Thielemann et al. (1986) SNIa yield models. These quantities are added to the existing oxygen and iron in the gas particles by mass and then converted to a fractional mass

of the gas particle so that when a new star forms, it will form with the same fractional metal content as its parent gas particle.

### 3.3 Stellar wind feedback

The feedback contribution of stellar winds is also significant. Stars with masses below  $\sim 8 M_{\odot}$  return substantial fractions of their mass to the ISM as they evolve and leave behind white dwarf remnants. We base our wind feedback on the work of Kennicutt et al. (1994) who find that the total stellar return fraction is 0.25 to 0.50 of the initial mass depending on the IMF. Because the return rate is so high, this form of feedback can greatly prolong star formation in galaxies without gas inflow.

For simplicity, we consider only stars between 1 and  $8 M_{\odot}$  and assume that lower mass stars remain unevolved. To determine the fraction of mass returned for a given stellar mass we use the initial-final mass relation of Weidemann (1987) and then fit his results to a continuous function.

In practical terms, we implement this feedback mechanism by first taking each star particle and determining the range of stellar masses that die during the current timestep using the lifetimes from Raiteri et al. (1996). Then we calculate a returned mass fraction for this mass range using the function derived from Weidemann (1987). We add the feedback to the gas particles in the same manner as the SNe feedbacks, except without injecting any energy. The metallicity of the returned gas is simply the metallicity of the star particle. In the future, we plan to include metal production by intermediate mass stars. The total fraction of mass lost from a star particle over  $>10$  Gyr is 40% and of this  $\sim 99\%$  of the mass loss results from stellar winds.

## 4 TESTS OF THE RECIPE

To closely examine our star formation formalism, we created an isolated model Milky Way (hereafter IMMW) based on the dynamical model presented in Klypin et al. (2002) at several different resolutions. We use these models to tune our star formation recipe to produce results consistent with observations (e.g. Rocha-Pinto & Maciel 1997; Kennicutt 1998; Wong & Blitz 2002).

### 4.1 Isolated Galaxy

The IMMW was created using the specifications of Springel (2000) in that it resides in a slightly modified Navarro et al. (1997) (hereafter NFW) dark matter halo where the central dark matter has been concentrated by infalling baryons. Thus, the density distribution and potential is slightly different from a pure NFW halo. We initially modelled the dark matter using a velocity  $v_{200}=150 \text{ km s}^{-1}$ , a concentration,  $c = r_{200}/r_s = 12$ , resulting in a mass  $M_{200} = 1.12 \times 10^{12} M_{\odot}$  and radius  $r_{200}=214 \text{ kpc}$  at an average overdensity  $\frac{\delta\rho}{\rho_c} = 200$ . However, to replicate as closely as possible the potential created in the Springel (2000) model, we fit a slightly different NFW profile to the particle potential. This fixed potential has  $M_{200} = 7.314 \times 10^{11} M_{\odot}$ ,  $r_{200}=153 \text{ kpc}$ , and concentration  $c=20.648$ .

The baryons are distributed in a stellar and gaseous

disk along with a spherical bulge that contains only star particles with a total baryonic mass of  $4.55 \times 10^{10} M_{\odot}$ . The bulge contains  $4.93 \times 10^9 M_{\odot}$ ,  $\sim 10\%$  the baryonic mass. The stellar disk follows an exponential profile with a scale length of 3.5 kpc and constitutes 90% of the total mass of the disk. We distributed the remaining 10% of the baryonic disk mass as collisional SPH gas particles in an exponential profile with a scale length of 7 kpc, twice the scale length of the stellar disk (Broeils & Rhee 1997). We introduce no holes or gaps in the gas because molecular gas studies show that where neutral atomic hydrogen column densities decrease in the inner parts of disks, molecular gas densities increase to fill the void (Wong & Blitz 2002).

We evolve the disk until the initial instabilities (caused by the initially smooth particle distribution developing a spiral pattern) die out before turning on star formation. The minimum Toomre Q value is 2, so this disk is a very stable disk and grows no bar.

To check whether our star formation rate converges to a single value at various resolutions, we replicate our model three times. The lowest resolution galaxy starts with only 9,000 star particles of  $5 \times 10^6 M_{\odot}$  and 2,000 gas particles of  $2.5 \times 10^6 M_{\odot}$ , the medium resolution galaxy has 45,000 star particles of  $1 \times 10^6 M_{\odot}$  and 10,000 gas particles of  $5 \times 10^5 M_{\odot}$ , and the highest resolution galaxy has 225,000 star particles of  $2 \times 10^5 M_{\odot}$  and 50,000 gas particles of  $1 \times 10^5 M_{\odot}$ . We soften the gravity using spline softening and our gravitational softening length, 650 pc for the gas particles and 325 pc for star particles, remains fixed for all three resolutions. The equivalent Plummer softening is about 0.7 times smaller.

## 4.2 Goals of IMMW

Many observations have been dedicated to studying star formation in the Milky Way and spiral galaxies similar to our IMMW. The observations allow us to constrain the values of our star formation recipe parameters. Schmidt (1959) provides the foremost constraint for how many stars should form in a dense gas environment. Schmidt showed that the surface density of star formation,  $\Sigma_{\text{SFR}}$ , follows a power law of the gas surface density,  $\Sigma_{\text{gas}}$ , called the Schmidt law. The more recent work of Kennicutt (1998) specifies the exact slope and normalisation of this relationship. Equation 4 of Kennicutt (1998) states that:

$$\Sigma_{\text{SFR}} = (2.5 \pm 0.7) \times 10^{-4} \left( \frac{\Sigma_{\text{gas}}}{1 M_{\odot} \text{pc}^{-2}} \right)^{1.4 \pm 0.15} M_{\odot} \text{yr}^{-1} \text{kpc}^{-2} \quad (12)$$

The formulation of our star formation recipe should ensure that our star formation approximately follows the slope of this relationship, while the star formation efficiency,  $c^*$ , should adjust the normalisation.

Another constraint is the observed nearly steady star formation rate in the Milky Way. The local stellar neighbourhood shows evidence that the star formation rate has been constant for Gyr (Rocha-Pinto & Maciel 1997) when averaged over long timescales. In our simulations, a steady star formation rate results from the maintenance of a constant exponential gas surface density profile. The Wong & Blitz (2002) observations of exponential gas surface density profiles, therefore, provide another constraint related to the steady star formation rate.

Our experiments consist of varying the four star formation criteria (temperature, density, converging flow, and Jeans) and the four parameters ( $c^*$ ,  $E_{\text{SN}}$ ,  $\beta$ , and  $\tau_{\text{CSO}}$ ) to determine how each criterion and each parameter affects star formation. Criteria are solid cutoffs that eliminate gas particles from forming stars whereas parameters are proportional constants that affect the rate of star formation and feedback. In this spirit, we choose a fiducial set of criteria and parameters, and then proceed to vary each parameter or criterion individually. Our fiducial criteria are  $T_{\text{max}} = 30,000$  K,  $n_{\text{min}} = 0.1 \text{ cm}^{-3}$ , flows must be converging, and no Jeans-like criterion. The fiducial parameters are  $\beta = 10,000$ ,  $c^* = 0.1$ ,  $\tau_{\text{CSO}} = 3 \times 10^7$  yr, and  $E_{\text{SN}} = 10^{50}$  ergs. These parameters do not necessarily represent a best fit, which is presented in the conclusions, but are simply a starting point that produce relatively normal results.

## 4.3 Numerical Precision

Our star formation recipe is implemented in the parallel tree SPH code GASOLINE (Wadsley et al. 2004). GASOLINE implements cooling similar to what is described in KWH. It assumes ionisation equilibrium, an ideal gas with primordial composition, and solves for the abundances of each ion species. The scheme uses the collisional ionisation rates reported in Abel et al. (1997), the radiative recombination rates from Black (1981) and Verner & Ferland (1996), bremsstrahlung, and line cooling from Cen (1992). The energy integration uses a semi-implicit stiff integrator independently for each particle with the compressive heating and density (i.e. terms dependent on other particles) assumed to be constant over the timestep.

Gravity is calculated for each particle using tree elements that span at most  $\theta = 0.7$  of the size of the tree element’s distance from the particle. Every particle has its forces calculated on each large time-step,  $1.53 \times 10^7$  yr. GASOLINE is multisteping so that every particle’s time-step  $\Delta t_{\text{grav}} = \eta \sqrt{\frac{\epsilon_i}{a_i}}$ , where  $\eta = 0.175$ ,  $\epsilon_i$  is the gravitational softening length, and  $a_i$  is the acceleration. For gas particles, the time-step must also be less than  $\Delta t_{\text{gas}} = \eta_{\text{Courant}} \frac{h_i}{c_i}$ , where  $\eta_{\text{Courant}} = 0.4$  and  $c_i$  is the sound speed. We restricted the smallest SPH smoothing length to be 0.01 of the gravitational softening length.

Stars are formed and feedback is calculated every 1 Myr in the simulations. The time between star formation events has no relationship to the major timesteps of the simulation when every particle has its forces calculated. However, star formation is tied to the minor timesteps when some subset of the particles have their forces calculated. As these timesteps may not be exactly 1 Myr, we choose the minor timestep that is closest to the time that we want to form stars and add feedback at that time.

## 5 RESULTS

We have conducted a variety of experiments with our IMMW, adjusting the parameters discussed above. For each of these experiments, we have data on the star formation

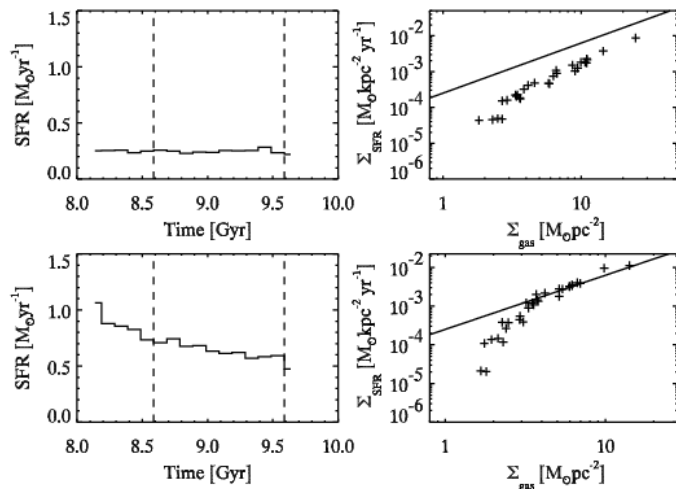


**Figure 2.** A demonstration of unacceptable (top) and acceptable (bottom) star formation conditions. The top panels are the results produced when using a small star formation efficiency,  $c^*$  of 0.01 in contrast to the bottom panels that use the best fit value of  $c^*=0.05$  in the blastwave model. The left panels plot the SFR vs. time and the right panels the SFR surface density vs. gas surface density relation. The two dashed lines in the left panel show the region that is used to calculate the average SFRs. The solid line in the right panel is the observed Schmidt Law (Kennicutt 1998).

rate (SFR) as a function of time and gas surface density<sup>1</sup>. In Figure 2, we present two parameter choices and show star formation histories and SFR surface density versus gas surface density relations as an example of star formation variation within our experiments. In this case, the blastwave feedback model is used in medium resolution (45,000 stars, 10,000 gas) IMMWs. The top panels are the results produced when using a small star formation efficiency,  $c^*$  of 0.01 in contrast to the best fit for the blastwave model  $c^*=0.05$  displayed in bottom plots.

The star formation history, plotted in the left panels, is a histogram of when stars formed. The vertical dashed lines indicate the period between  $6 \times 10^8$  and  $1.6 \times 10^9$  yr after the beginning of the simulation, the time over which we calculate the average SFR, which we use in subsequent plots. The simulations start 8 Gyr after the stars in the initial conditions formed so that there are no feedback effects from those stars. We choose a time period past the beginning of the simulation because it falls well after any initial transient starburst that may result from non-equilibrium initial conditions. Such a starburst can happen because all the gas particles at the start of the simulation are unaffected by feedback and hence all of them may be eligible to form stars. As shown in the panels, both choices result in an approximately constant star formation history but the amount of present day star formation in the upper panel is lower than the observed value.

The right panels of Figure 2 show SFR surface density versus gas surface density and indicates how well our star formation follows a Schmidt law (Kennicutt 1998). To create these plots, we azimuthally sum the mass of stars that

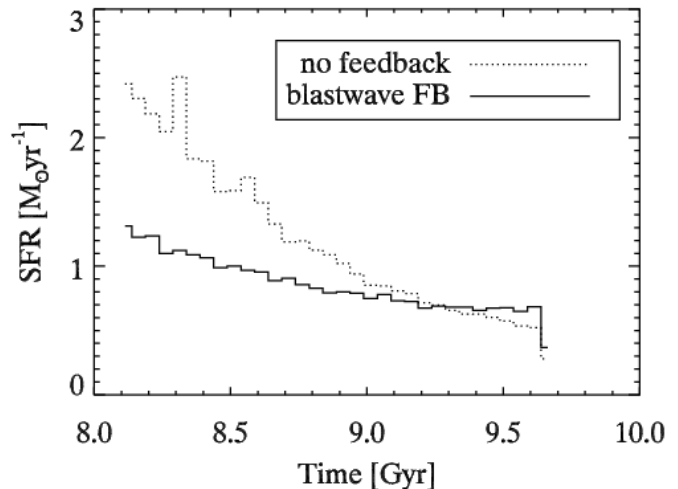


**Figure 3.** A comparison between star formation with (solid) and without (dotted) feedback. The run with feedback uses  $E_{\text{SN}} = 3 \times 10^{50}$  ergs with the blastwave model at high resolution (275,000 particles).

formed over the last 100 Myr of the simulation in 500 pc radial bins and plot them against the final surface density of the gas in each bin. The panels show that our star formation formulation creates a Schmidt Law with the right slope. However, the upper panel does not have the correct amplitude suggesting that the choice of parameters was incorrect. It is generally the case that an average star formation rate of around  $0.8 M_{\odot} \text{ yr}^{-1}$  in the high resolution case reproduces the Schmidt Law in the IMMW experiments. The turn down in SFR density at surface densities less than  $2 M_{\odot} \text{ pc}^{-2}$  matches the observations of Martin & Kennicutt (2001) as we discuss in Section 6.3.

The effect of feedback is previewed in Figure 3 from a high resolution (225,000 stars, 50,000 gas) IMMW. The shallower drop-off in star formation rate with feedback owes in part to the fact that the supernova energy is being effectively used to prevent star formation and in part due to the stellar wind feedback that returns gas to the ISM. Both star formation rates decline exponentially because of the stochastic recipe (§2.2). Figure 4 shows how the feedback immediately increases the temperature of the gas surrounding stars that have recently formed. The higher temperature results in higher pressure that allows the hot particle to push around the cooler gas surrounding it, as shown in Figure 19. The expansion leads to only a modest reduction in density because density is a smoothed property that includes the surrounding high density particles. Thus, it is not low gas density that suppresses star formation, but high gas temperature.

## 5.1 Effects of Criteria

### 5.1.1 $T_{\text{max}}$ : Maximum Temperature

As we already stated, we added an additional criterion to those in Katz (1992) and KWH: gas particles may not form stars unless their temperature is below  $T_{\text{max}}$ , typically 10,000's K. This may seem like a high temperature threshold for star formation given that star forming molecular clouds are observed to cool down to  $\sim 100$  K. However, our cooling

<sup>1</sup> <http://hpcc.astro.washington.edu/feedback>

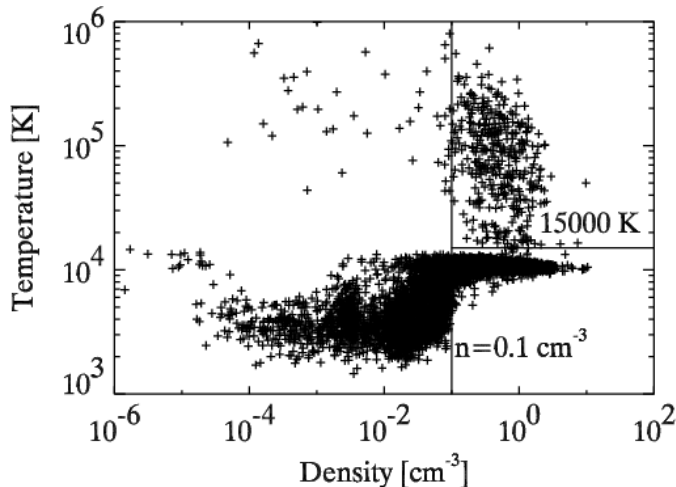


**Figure 4.** The phase diagram for the 50,000 gas particles in the high resolution (275,000 particles) IMMW run with  $E_{\text{SN}} = 3 \times 10^{50}$  ergs using the blastwave model. The fiducial values for  $T_{\text{max}}$  and  $n_{\text{min}}$  are drawn to indicate the gas particles that pass the star formation criteria. All of the particles with temperatures above 15,000 K are there as a result of feedback because all gas particles in the disk start with  $T=10,000$  K. A couple of gas particles show a modest decrease in density below the density threshold indicating that the gas does expand slightly owing to its high temperature and pressure.

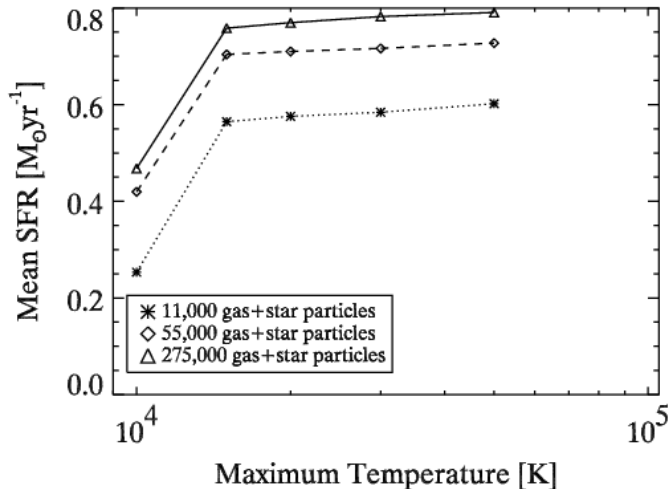


**Figure 5.** The mean SFR as a function of  $T_{\text{max}}$  at low resolution (asterisks), medium resolution (diamonds), and high resolution (triangles).

is limited to H and He atomic cooling, which can only cool gas down to  $\sim 10,000$  K, and we average over scales much larger than star forming clouds. A future improvement to the code will be to include molecular hydrogen cooling (e.g. Abel et al. (1997) and Kravtsov (2003)), which will allow the gas to cool below 10,000 K, but even then, unless the resolution were greatly improved,  $T_{\text{max}}$  should remain above 10,000 K.

Figure 5 shows the effect that varying  $T_{\text{max}}$  from 10,000–50,000 K has on the mean SFR. As long as  $T_{\text{max}} \gtrsim 15,000$

K the mean SFR is almost independent of  $T_{\text{max}}$ . We might expect so little effect since most gas particles that are near star forming temperatures have cooled all the way to 10,000 K. For example, only 18% of the gas mass in the medium resolution simulation, and only 20% of the gas mass at high resolution is warmer than 12,000 K after 1 Gyr of evolution using our fiducial recipe. It is only those gas particles that have been heated as the result of supernova feedback that are excluded from forming stars by the  $T_{\text{max}}$  criterion even though they may remain in a dense environment. We tried lowering the threshold temperature all the way down to the mean gas particle temperature, 10,000 K. This produced galaxies with much burstier star formation histories. Gas particles would pile up just above the temperature threshold, cool all at once, produce lots of star formation, and then heat the gas up so that it could not form stars until the next cooling episode started the cycle all over again. This experiment demonstrates that  $T_{\text{max}}$  should stay above 12,000 K, but its specific value does not critically affect star formation. We choose to use  $T_{\text{max}} = 15,000$  K. We note that the  $T_{\text{max}}$  criterion is critical to our feedback prescription because it enables star formation to be immediately suppressed by supernova feedback.

### 5.1.2 $n_{\text{min}}$ : Minimum Density

As  $n_{\text{min}}$  increases, fewer gas particles are eligible to form stars, and hence fewer stars form. Figure 6 shows that a hundred-fold increase in the minimum density causes an order of magnitude reduction in the star formation rate. As the gas density profile declines exponentially, most of the gas particles that are not eligible to form stars reside in the outer parts of the disk. Because the IMMW disk is gravitationally stable, instabilities do not drive star formation and thus density simply correlates with radius. The minimum density that we choose,  $0.1 \text{ cm}^{-3}$ , confines star formation the inner 20 kpc of our model galaxy, which corresponds to surface densities of approximately  $2M_{\odot} \text{ pc}^{-2}$  and above and matches the observed minimum density threshold for star formation in nearby spiral galaxies (Martin & Kennicutt 2001).

### 5.1.3 Jeans Criterion

The Jeans Criterion (§2.1) is a test of whether or not a gas cloud can provide enough pressure support to prevent gravitational collapse and is commonly used to test whether gas can form stars. Our initial recipe implemented it as a comparison between the sound crossing time,  $h_i/c_i$ , where  $h_i$  is the smoothing length and  $c_i$  is the sound speed, and the dynamical time,  $1/\sqrt{4\pi G\rho_i}$ .

Figure 7 shows this comparison for all the gas particles in the simulation at three different resolutions. What is immediately apparent is that the sound crossing time decreases significantly with increasing resolution, which happens because a region at given density is sampled by more particles in the higher resolution simulations. More resolution, without a corresponding drop in temperature, results in a smaller smoothing length making the sound crossing time shorter. This decrease in the sound crossing time becomes significant enough in the highest resolution simulation to make

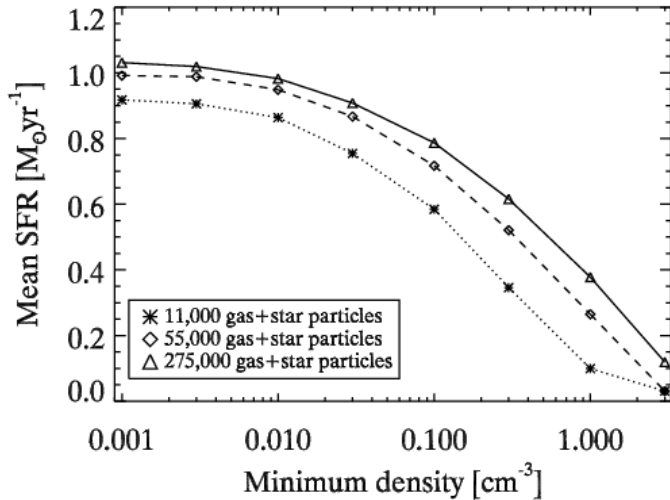


**Figure 6.** The mean SFR as a function of minimum density ( $\rho_{\min}$ ) at low resolution (asterisks), medium resolution (diamonds), and high resolution (triangles).

gas particles unable to pass the Jeans Criterion, at least using our formulation of it and the atomic transition cooling function employed in these simulations. We also plot a line representing particles at 9500 K in the high resolution simulation, as cold as they can get using atomic cooling, using typical smoothing lengths, which shows that typical particles have little chance of passing the Jeans Criterion unless they cool a great deal adiabatically. Gas at the highest densities is sampled at the highest resolution but because the gas does not realistically cool, the sound crossing time becomes so short that  $t_{\text{dyn}}$  is still greater than  $h_i/c_i$ , and the dense gas unrealistically fails the Jeans Criterion. This might not be true if we included more realistic molecular cooling.

We plot the star formation histories obtained when we include the Jeans Criterion in Figure 8. The consequences of this problem are evident as few stars are able to form in the highest resolution simulation. Thus, we reject using the Jeans Criterion and use the simpler collapse conditions imposed by requiring that the gas have a minimum density and a maximum temperature.

Ideally the simulations would also include molecular cooling so that particles would have more realistic temperatures, making the Jeans Criterion a more appropriate test. Figure 7 shows how the cooling curve used in these simulations can only cool particles down to 9500 K at high resolution. Any further decrease in temperature is the result of adiabatic cooling. Figure 7 also shows how the temperature maximum plays a similar role to the Jeans criterion. However, the limit changes with resolution in this plot because the sound crossing time decreases with decreasing smoothing length while the sound speed of 15,000 K gas remains constant. For clarity, we only plot the high resolution maximum temperature limit. In the current generation of simulations of forming galaxies, the models only attempt to replicate the generic properties of star formation that seem to be well represented by a Schmidt Law as observed by Kennicutt (1998). A temperature maximum of  $T_{\text{max}}=15,000$  K ensures that only reasonably cool gas particles form stars. The stochastic implementation of the star formation formula ensures the

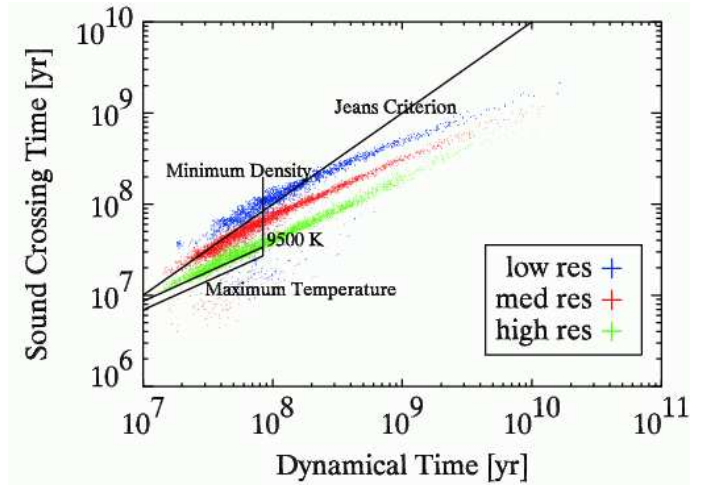


**Figure 7.** The sound crossing time across a smoothing length versus the local dynamical time for 3 different simulation resolutions. An increase in resolution, which decreases the smoothing lengths and hence the sound crossing times takes gas particles from satisfying the Jeans Criterion in low resolution simulations (blue points) to failing the criterion in high resolution runs (green points) because the atomic cooling included in these simulations only allows gas to cool to 10,000 K. The line for particles at 9500 K uses typical smoothing lengths of 360 pc at  $0.1 \text{ cm}^{-3}$  ( $t_{\text{dyn}} \sim 80 \text{ Myr}$ ) and 92 pc at  $6 \text{ cm}^{-3}$  ( $t_{\text{dyn}} = 10 \text{ Myr}$ ). We also plot the maximum temperature criterion for the high resolution simulation.

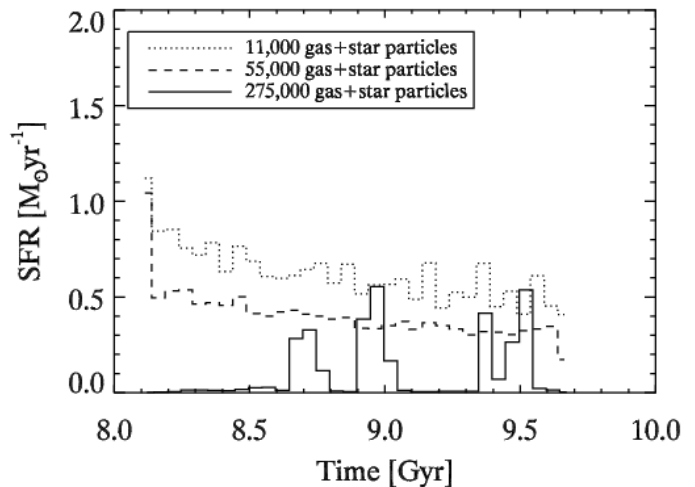


**Figure 8.** The mean star formation rates at three different resolutions when the Jeans criterion is enabled. While the low (dashed) and medium (dotted) resolution simulations form a similar number of stars, star formation is nearly eliminated in the high resolution (solid) simulation except for a couple of bursts.

correct slope and with  $n_{\min}=0.1 \text{ cm}^{-3}$  we reproduce the correct low density threshold, making a Jeans criterion unnecessary.

#### 5.1.4 Converging flow

Most of the particles that satisfy the temperature and density criteria also satisfy the criterion that the flow be converging. Therefore, there is not a large difference in the number of stars formed in our IMMW galaxy with the criterion turned on or off. The difference was minor enough that we decided to run all of the simulations reported in this paper with the converging flow criterion enabled since it might still be of benefit in nonequilibrium situations that we will explore in future work.

#### 5.1.5 Summary of Criteria

The criteria that we settled on are:

- The gas particle must be colder than  $T_{\max} = 15,000$  K.
- The gas particle must be denser than  $n_{\min} = 0.1 \text{ cm}^{-3}$ .
- The gas particle must be overdense enough to be part of a virialised structure.
- The particle must be part of a converging flow, i.e.  $\nabla \cdot \mathbf{v} < 0$ .

In addition we found that the Jeans Instability loses meaning at high resolution as it is formulated in Katz (1992) and that star formation is most sensitive to the  $n_{\min}$  criterion.

## 5.2 Effects of Parameters in the $\beta$ Model

The criteria established in the above section are appropriate for either of our feedback schemes. In this section we discuss how parameter choice affects star formation in the  $\beta$  recipe (§3.1.1). For all of these simulations, we used our fiducial choices and changed only the specified parameter to measure its effect on the star formation.

### 5.2.1 $\beta$ : Supernova Feedback Mass Factor

The  $\beta$  parameter distinguishes our method from those used by Gerritsen (1997) and Thacker & Couchman (2001). Gerritsen (1997) turns off the radiative cooling only for one gas particle while Thacker & Couchman (2001) turn off the radiative cooling for all 32 particles within the smoothing radius. The  $\beta$  model gives us more flexibility. For example, turning off the cooling for all 32 neighbouring gas particles could produce a feedback that is too strong and resolution dependent. In a low resolution simulation, the smoothing length is much longer than in a high resolution simulation, so much more gas is affected and the feedback is stronger. However, this effect is mitigated to a certain extent since the star particles are more massive, so that the feedback is the result of more supernovae explosions. Another possible problem is that disabling the cooling for all 32 particles does not take into account how much energy has been released in the supernova explosions. Even if only one supernova explodes, it has the same effect as if hundreds of supernova exploded.

As expected, Figure 9 shows that the more gas particles that have their radiative cooling disabled, i.e. larger values of  $\beta$ , the fewer stars form, because the gas particles are not able to satisfy the maximum temperature criterion. Once  $\beta$  becomes large enough such that all the 32 neighbouring

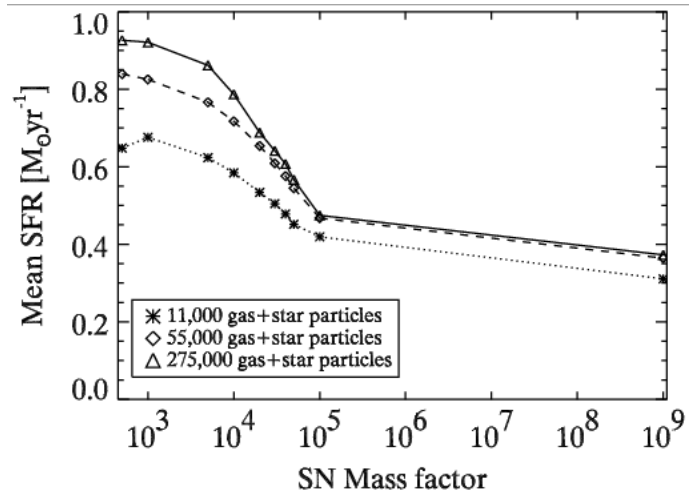


**Figure 9.** The star formation rate as a function of mass factor  $\beta$  at low resolution (asterisks), at medium resolution (diamonds), and at high resolution (triangles).

gas particles that received supernova feedback energy have their cooling disabled, increasing  $\beta$  further has little additional effect. The reduced star formation at very low  $\beta$  (the leftmost lowest resolution point in Figure 9) occurs because our analysis averages star formation after the initial burst where much of the gas is converted into stars leaving little gas to form stars at later times.

Figure 10 shows the details of the  $\beta$  feedback model and can be compared with similar plots for the blastwave model shown in Figure 18. The plots show the results using the fiducial recipe with  $\beta = 10,000$ . The critical panel is in the upper, right-hand corner where we plot how many gas particles have their cooling disabled for each star particle during a given star formation event. One can see that the number of particles affected is not resolution dependent. Star particles produce an amount of SN energy proportional to their mass (as in the upper-left panel of Figure 18) and, therefore, one might expect the radii within which we disable the cooling to be larger for lower resolution simulations. However, the inter-particle separation also changes with resolution and thus the blastwave regions are proportionally the same size as shown in the lower left hand panel. Here we normalise the radii to the high resolution simulation by scaling with the mass in supernova to the one third power. To recover the actual radii, in the medium resolution simulation just multiply by 1.6 and in the low resolution simulation by 2.7. But since the  $\beta$  model does not take into account how blastwaves expand differently in different density environments, the blastwave model provides a more physical representation of supernova explosions as described in §3.1.2.

### 5.2.2 $\tau_{\text{CSO}}$ : Cooling Shutoff Time

We choose our fiducial  $\tau_{\text{CSO}} = 30$  Myr, the time that we disable the radiative cooling, based upon Gerritsen (1997) and Thacker & Couchman (2000). Figure 11 shows that there is not a significant increase in the SFR as  $\tau_{\text{CSO}}$  decreases. We prefer a short  $\tau_{\text{CSO}}$  as it more closely matches the expected lifetime of SN blastwaves.

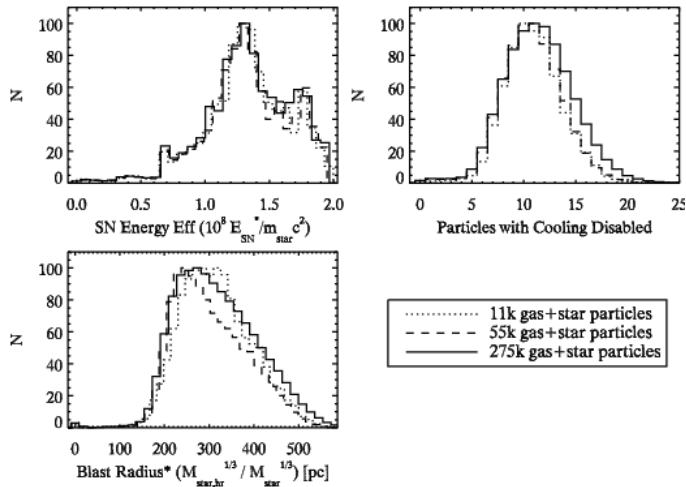


**Figure 10.** Detailed characteristics of supernova feedback in the  $\beta$  model for three different resolution simulations with the parameters set at their fiducial values. Each resolution has widely varying particle numbers, so every histogram has been normalised to a maximum of 100. The statistics were compiled over the first 200 Myr of the simulation. The upper-left panel plots the distribution of energies that each star particle releases from supernova explosions every time supernova feedback is calculated (1 Myr). That quantity is normalised using star particle rest mass energies ( $E_{\text{SN}}^*/m_{\text{star}}c^2$ ) to make comparisons between resolutions easier. We note that the quantity  $E_{\text{SN}}^*$ , the energy the entire star particle releases into the ISM, is different than the quantity  $E_{\text{SN}}$  used elsewhere in this paper for the energy that individual supernovae release into the ISM. Effectively, the normalised quantity represents the efficiency with which the matter in the star particles are converted into energy. The upper-right panel plots the number of particles with their cooling disabled. The relationship between gas particle mass and resolution means that the number of particles with cooling disabled roughly traces the gas mass with cooling disabled, which is similar for every resolution. The lower-left panel plots the distribution of radii within which the cooling is disabled renormalised to the high resolution simulation by scaling by the mass in supernova to the one third power.

### 5.2.3 $c^*$ : Star Formation Efficiency

$c^*$  controls the efficiency with which stars form. The  $c^*$  parameter can be thought of as either modifying the timescale for star formation (Springel & Hernquist 2003) or as the fraction of gas that becomes stars. The distribution of star formation timescales,  $t_{\text{form}}$ , for gas particles that pass the star formation criteria is close to a log normal distribution with a peak around 20 Myr and a tail out to 80 Myr. The results are plotted for our fiducial values at medium resolution and the times range from 20 to 80 Myr. Remember that  $t_{\text{form}} = t_{\text{dyn}} = 1/\sqrt{4\pi G\rho}$  so the times just trace the gas density. Our fiducial value of  $c^* = 0.1$  either corresponds to star formation timescales of  $\sim 300$  Myr or implies that  $\frac{1}{10}$  of a gas particle gets converted to stars each star formation timescale,  $\sim 30$  Myr.

Figure 12 shows that  $c^*$  has the strongest effect on star formation of any of the parameters that we have investigated so far. The value for  $c^*$  is thus tightly constrained using the Schmidt Law (Kennicutt 1998) defined in Equation 12 and the best fit for the  $\beta$  feedback model is with  $c^* \sim 0.1$ .

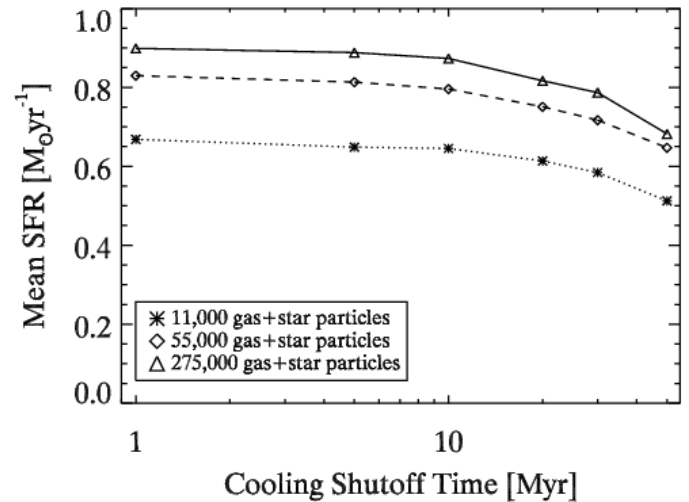


**Figure 11.** The mean SFR as a function of the time that radiative cooling is disabled at low resolution (asterisks), at medium resolution (diamonds), and at high resolution (triangles).

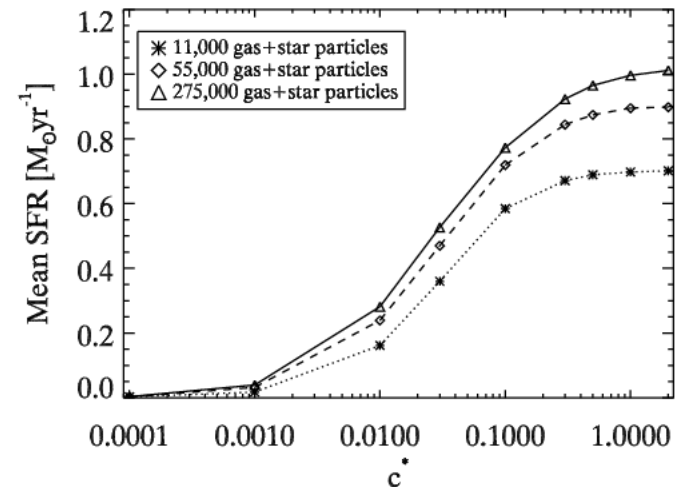


**Figure 12.** The mean SFR as a function of  $c^*$  at low resolution (asterisks), at medium resolution (diamonds), and at high resolution (triangles).

### 5.2.4 $E_{\text{SN}}$ : Supernova Energy

During the late stages of its life, the core of a massive star possesses  $10^{53}$  ergs of gravitational potential energy. How much of that energy is converted into thermal energy in the surrounding interstellar medium during a Type II SN explosion remains an open question. Most of the energy is converted into neutrinos and a small fraction of the neutrino flux interacts with enough matter to provide the canonical SN kinetic energy value of  $10^{51}$  ergs (Colgate & White 1966). Integrating SN light curves reveals that only  $10^{49}$  ergs are radiated away in the initial explosion (Filippenko 1997), but it is not clear that the rest of the energy is transferred to the ISM. In the current recipe, we have chosen to leave the energy transfer efficiency as a parameter,  $E_{\text{SN}}$ , and use the Thornton et al. (1998) estimate that 10% of the supernova's kinetic energy is converted into thermal energy as

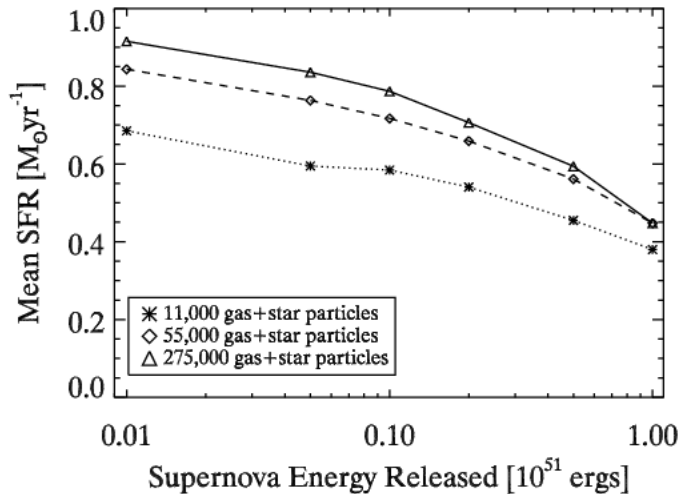


**Figure 13.** The mean SFR as a function of  $E_{\text{SN}}$  using the  $\beta$  feedback model at low resolution (asterisks), at medium resolution (diamonds), and at high resolution (triangles).

our fiducial value. The rest of the energy is radiated away throughout the lifetime of the supernova blastwave.

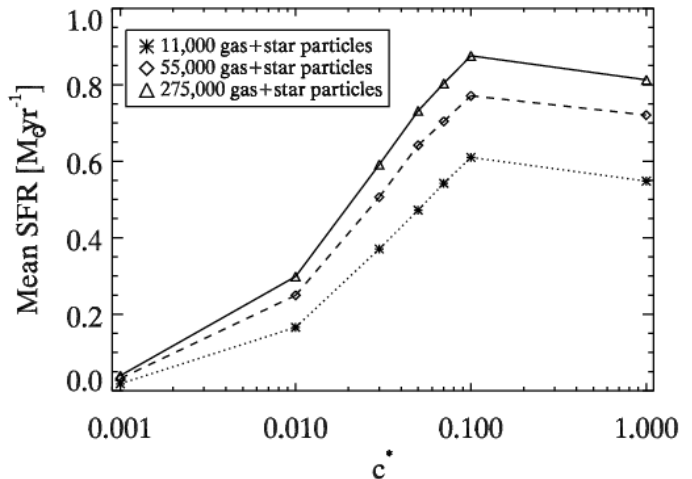
We distribute the supernova energy across all 32 nearest neighbour particles using the smoothing kernel. Since we are only disabling the cooling in a limited set of those particles, some of the energy will be quickly radiated away and have no effect on the simulation. However, the majority of the energy goes to particles that do have their radiative cooling disabled and thus the feedback does effect star formation.

Figure 13 shows that more stars form when less supernova energy is returned to the ISM, as one would expect. All of the  $E_{\text{SN}}$  values came close to fitting the Schmidt Law, with  $2 \times 10^{50} < E_{\text{SN}} < 6 \times 10^{50}$  doing the best.  $E_{\text{SN}}$  does not have its largest impact on star formation in our IMMW. Its value is better constrained using other observables (see §6.1) or smaller galaxies. The reason that  $E_{\text{SN}}$  effects SFRs for the IMMW is that gas particles get heated more when  $E_{\text{SN}}$  is increased and thus are less likely to fall below the  $T_{\text{max}}$ . The gas may also expand more owing to the additional pressure and be less likely to satisfy the  $n_{\text{min}}$  criterion. We note that the star formation rate begins to converge to one mean SFR as  $E_{\text{SN}}$  approaches  $10^{51}$  ergs.

### 5.3 Effects of Parameters on the Analytic Blastwave Model

The results of the previous section proved that turning off the radiative cooling of gas particles is an effective means of implementing supernova feedback in our IMMW. The results also show that shorter  $\tau_{\text{CSO}}$  and moderate  $\beta$  values are in good agreement with the analytic blastwave solutions presented in McKee & Ostriker (1977). Using these analytic expressions (detailed in §3.1.2) leaves only two free parameters,  $c^*$  and  $E_{\text{SN}}$ , governing both star formation and feedback and is well motivated physically.

The results of two different versions of the blastwave model are presented below. First, supernova feedbacks, i.e. thermal energy, metals, and mass, are distributed across the entire smoothing radius as described in §5.3.1. However,



**Figure 14.** The mean SFR as a function of  $c^*$  at three different resolutions using the blastwave model and smoothing over 32 particles for simulations at low resolution (asterisks), at medium resolution (diamonds), and at high resolution (triangles).

since energy that is added to particles that can cool is lost almost immediately we propose a second variant where we concentrate the feedback to only those particles that have their cooling disabled as we describe in §5.3.2.

#### 5.3.1 Smoothing over 32 Particles

The star formation efficiency,  $c^*$ , has a large effect on star formation when we use the analytic blastwave model much like in the  $\beta$  model as we show in Figure 14. Most values of  $c^*$  do not reproduce the observed Schmidt Law; only  $c^*=0.05$  gives the Kennicutt (1998) normalisation at all three resolutions. Therefore, every simulation described hereafter uses  $c^* = 0.05$  as its fiducial value.

As discussed in §3.1.2, there are two possible shutoff times in the blastwave method,  $t_E$ , the time that the snowplow phase ends, and  $t_{\text{max}}$  the time that it takes the gas to cool down to the ambient ISM temperature. We find that in the IMMW simulations there is little difference in the SFR between the two different choices with each having a SFR of  $0.8 M_{\odot} \text{ yr}^{-1}$  at high resolution with  $c^* = 0.05$ .

The amount of supernova energy transferred to the ISM has little effect on star formation as shown in Figure 15. All of the values of  $E_{\text{SN}}$  using  $c^* = 0.05$  fit the observed Schmidt Law well. Supernova energy provides local feedback and this maintains a steady SFR, but the amount of energy does not have a huge impact on the amount of star formation.

#### 5.3.2 SN Ejecta Smoothed only over the Blast Radius

In our effort to inject the energy from supernovae ejecta into the ISM both efficiently and more physically, we concentrate the energy into just those particles inside of the blast radius, i.e. those that will have their cooling disabled when SNIa explode. We also concentrate the energy and metal deposition for SNIa as a matter of convenience, but do not disable radiative cooling for gas particles that are only within the SNIa blast radius. When there are no gas particles inside the

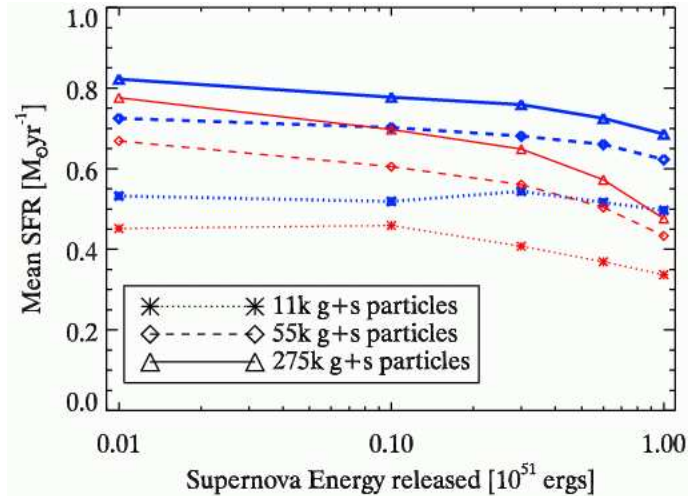


**Figure 15.** The mean SFR as a function of supernova energy for the blastwave feedback model with smoothing over 32 particles (thick, blue) and when the feedback is concentrated (thin, red) at low resolution (asterisks), at medium resolution (diamonds), and at high resolution (triangles).

blast radius, as often occurs when for stellar wind feedback, we deposit all of the energy into the nearest gas particle.

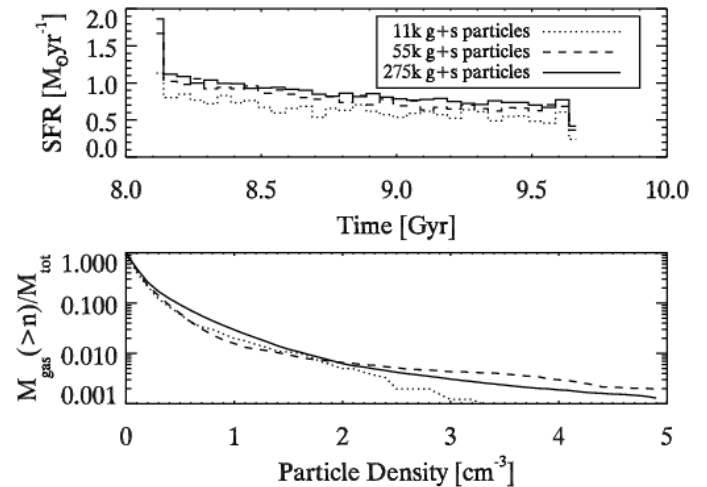
Concentrating the ejecta inside the blast radius has an impact on star formation. The average star formation rate drops to  $0.7 M_{\odot} \text{ yr}^{-1}$  at  $c^*=0.05$  and  $E_{\text{SN}} = 10^{50}$  ergs for the high resolution simulations from the  $0.8 M_{\odot} \text{ yr}^{-1}$  shown previously. While the star formation decreases, the shape of the star formation history does not change.

Figure 15 shows how the mean SFR decreases more when the energy is concentrated within the blast radius as opposed to spreading it over all 32 neighbouring particles. However, the variation in mean SFR does not lead to any deviation from the Schmidt Law, so it is not possible to constrain the value of  $E_{\text{SN}}$  from star formation in the IMMW alone.

#### 5.4 Effects of Resolution

One trend that is apparent from all the plots is that more stars form at higher resolution. With the fiducial recipe, there is a factor of two difference in SFRs between the lowest resolution simulation with 11,000 particles and the highest resolution simulation with 275,000 particles. There is a smaller difference between the medium and high resolution simulations than there is between the low and medium resolutions so perhaps the results are converging. But a factor of two remains a significant impediment to comparing simulations with observations.

The difference in star formation is caused in part by the higher densities that gas particles reach in higher resolution simulations. Denser gas forms more stars because of Equation 4. The bottom panel of Figure 16 shows that the most critical density range is between  $0.5$  and  $1.5 \text{ cm}^{-3}$ . Most of the star forming eligible gas mass falls in this range and there is a significant difference in the fraction of gas with these densities. In the high resolution simulation two times more gas has these densities than in the low resolution sim-



**Figure 16.** The top panel shows how the SFR formation rate as a function of time increases with increasing resolution for the fiducial parameter settings of the  $\beta$  model at three different resolutions. The bottom panel is a cumulative plot of gas mass fraction at various densities and shows why the SFR increases, as a greater fraction of gas is at star forming densities in the higher resolution simulations.

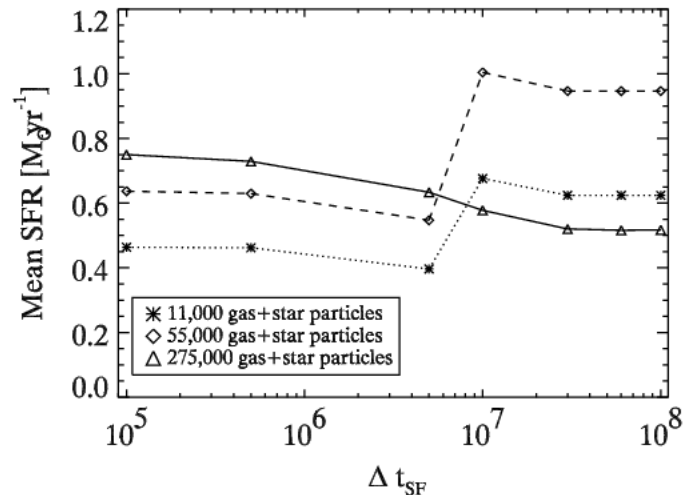


**Figure 17.** The mean SFR as a function of the timestep used for star formation,  $\Delta t_{\text{SF}}$ , for the fiducial blastwave model at low resolution (asterisks), at medium resolution (diamonds), and at high resolution (triangles).

ulation. There are smaller fractions of gas at high density and Figure 16 shows that the different resolutions vary randomly in their high density gas mass content. The top panel of Figure 16 shows that these variations have little bearing on how many stars form.

Time resolution can also affect the SFR; we calculate star formation every  $\Delta t_{\text{SF}}$ . Our value of  $\Delta t_{\text{SF}} = 1 \text{ Myr}$  comes from considering the fact that O star lifetimes can be as short as 1 Myr. Figure 17, however, shows that the actual value of  $\Delta t_{\text{SF}}$  is not crucial until either it starts to approach the time over which we disable the cooling, calculated using the analytic blastwave solution, which is typically around 10

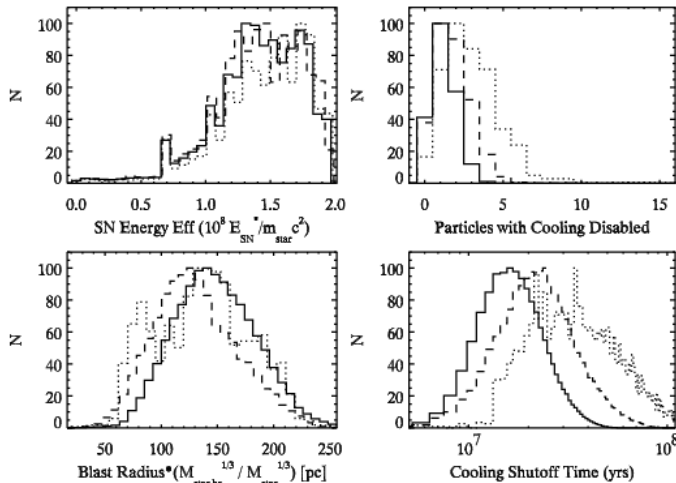


**Figure 18.** The same as Figure 10 for the blastwave feedback model where all the feedback is concentrated within the blast radius. There is one additional panel in the lower right where we plot the distribution of the cooling shutoff times.

Myr, or the length of a major system timestep, 15.6 Myr in these simulations. As star formation and feedback are not computationally intensive, calculating it every Myr is practical and will not adversely affect star formation.

#### 5.4.1 Feedback Behaviour

The feedback method also contributes to the resolution sensitivity. As in the  $\beta$  method, more particles have their cooling disabled when the blastwave recipe is used at low resolution than at higher resolution as shown in Figure 18. The radial extent of the blastwave depends on the energy of the explosion, so the bigger star particles in the low resolution simulation generate a larger effect than the larger number of star particles in the higher resolution simulations. However, also like in the  $\beta$  method, the differences disappear if one rescales by the mass in supernova to the one third power. The length of time that we disable cooling does depend on the resolution, i.e. the cooling is disabled for longer periods at lower resolution. This is because supernova feedback events are larger but less frequent at lower resolution. At any one time there is about the same amount of gas mass with its cooling disabled at all three resolutions. It should be noted that Figures 9, 11, 13, and 15 show that star formation converges as the amount of feedback increases. Unfortunately, these values for the feedback are unphysical and produce fewer stars than observed.

## 6 DISCUSSION

### 6.1 Constraints

The Kennicutt (1998) and Martin & Kennicutt (2001) observations provide three constraints on how the star formation rate relates to the gas surface density. The first is that the logarithmic slope is  $1.4 \pm 0.2$  and constrains us to use the stochastic formulation of star formation where

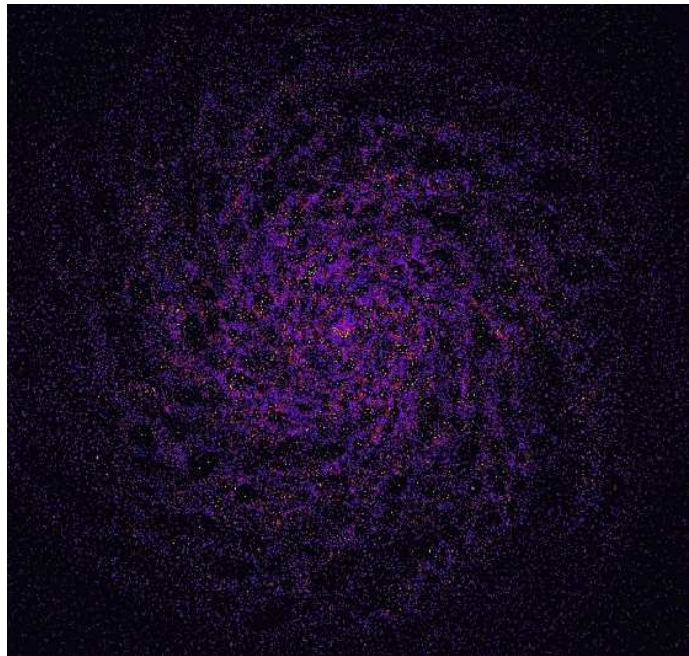


**Figure 19.** An example of the effect that supernova feedback has on the structure of our IMMW. The figure measures 24 kpc on a side. Notice the hot, yellow particles that have pushed the colder, more purple particles more in the low density outer regions of the galaxy and less in the dense, inner regions.

$SFR \sim \rho/t_{\text{dyn}}$ . The second is the normalisation of that relation. Using the  $\beta$  recipe, there are many different parameter combinations that can produce the proper normalisation. Using the blastwave method, only  $c^*$  greatly influences the star formation rate and  $c^*=0.05$  fits the Kennicutt (1998) observations the best. Finally, there is the low density cut-off observed by Martin & Kennicutt (2001), which we reproduce with our  $n_{\text{min}}$  criterion of  $0.1 \text{ cm}^{-3}$ .

The observations of Rocha-Pinto & Maciel (1997) indicate that stars have formed at roughly a constant rate for some time in the Milky Way based on the metallicity of G dwarfs. In the isolated model Milky Way (IMMW) star formation stays relatively constant with a slow decay when feedback is enabled. Figure 3 of Rocha-Pinto & Maciel (1997) provides no conclusive evidence of whether or not the star formation rate declines significantly. The major difference between our simulations and the Milky Way is that the IMMW is isolated. It has no external source of gas like the real Milky Way, which may be in the form of gas rich mergers or cold gas streaming in along filaments, and it is not gravitationally disturbed by the presence of orbiting satellites.

Figure 19 shows that our feedback method produces hot gas particles that push the cold gas into dense filaments where the gas particles are cool and dense enough to form stars. The holes that the SN blow open are smaller in the dense centre of our IMMW and grow progressively larger as the SN explode in the less dense regions in the outskirts of the galaxy. Images of the Large Magellanic Cloud in HI show similar features (see Figure 4 of Jones et al. (1999) or Figure 3 of Kim et al. (2003) for a similar image of the Circinus Galaxy). Inside of the Milky Way disk, Hartmann

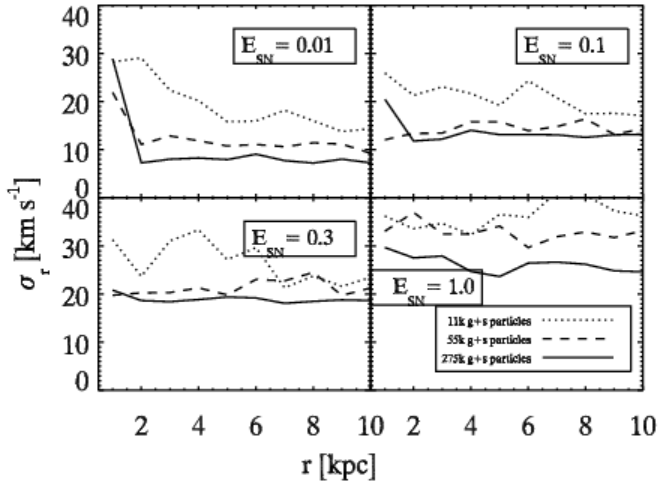


**Figure 20.** The radial velocity dispersion vs. radius of the gas particles in our concentrated blastwave model for four choices of the supernova feedback energy,  $E_{\text{SN}}$  at the three resolutions. We calculate the dispersion within 10 evenly spaced, radial bins between 0 and 10 kpc. The dispersion is most accurately determined for the highest resolution simulation (solid line).

(2002) observes that star formation happens along filamentary structures. Because of the jostling provided by the adiabatic expansion of supernova heated gas, the site of star formation is constantly shifting from one high density region to the next high density region. Our simulations are not run with enough resolution to follow the fine turbulence and shockwaves that lead to star formation, but do show structures that are reminiscent of what is observed.

We cannot use star formation properties to constrain the one free parameter in the blastwave feedback method, the amount of energy per supernova,  $E_{\text{SN}}$ , because in simulations of the IMMW the SFR is not very sensitive to changes in  $E_{\text{SN}}$ . To constrain this parameter we use the radial velocity dispersion of the gas in the disk plane and the mass fraction of gas in the hot phase. In Figure 20 we plot the radial velocity dispersion of the gas versus radius for the three resolutions using four different values for  $E_{\text{SN}}$ . The dispersions are almost independent of radius as observed in spiral galaxies. They are higher for the lowest resolution simulation but similar for the two highest resolutions. As expected the dispersion increases with the energy of the feedback. Typical vertical velocity dispersions of gas (under the assumption that random gas motions are isotropic) measured in quiescent spiral galaxies are a little more than 10 km s<sup>-1</sup> (Dickey & Lockman 1990; Dickey et al. 1990), so we prefer  $E_{\text{SN}} \sim 10^{50}$ .

In Figure 21 we plot the cumulative mass fraction of gas above a given temperature. We plot this at all three resolutions for the same four choices of  $E_{\text{SN}}$  as in Figure 20. The temperature mass fractions are almost independent of resolution except for the temperature of the hottest gas in the two cases with the smallest supernova feedback. In these two plots the higher the resolution the hotter the gas can become. More importantly, the fraction of gas in the cold star forming phase is very similar across the three resolutions. As expected, when the supernova feedback energy becomes

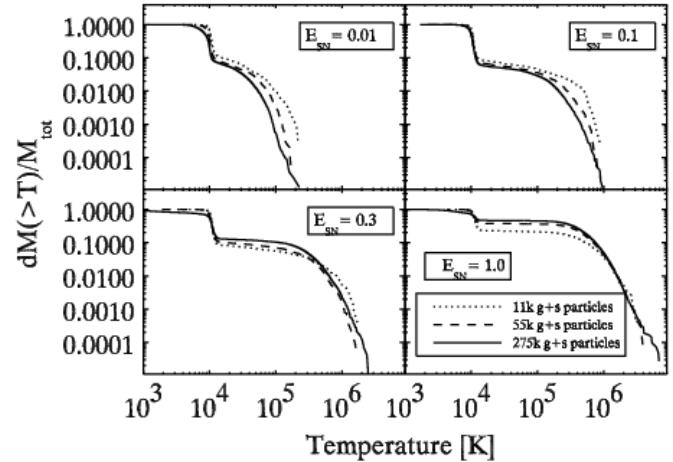


**Figure 21.** The cumulative mass fraction of gas above a given temperature for the blastwave method using four different supernova feedback energies,  $E_{\text{SN}}$  at each of the three resolutions.

larger, the gas can become hotter and a smaller fraction of gas remains in the cold phase. Early soft x-ray observations (Gorenstein et al. 1974; Burstein et al. 1977) and observations of the O VI absorption line (Jenkins & Meloy 1974; York 1974) placed limits on the mass fraction of hot gas in the Milky Way with a temperature greater than  $5 \times 10^5$  K. Hot gas mass makes up  $\sim 0.01$  of the ISM (van der Hulst 1996). Since the dispersion preferred value of  $E_{\text{SN}} = 10^{50}$  agrees with these observations, we fix the supernova energy at this value.

## 6.2 Live Halo

All the simulations reported so far have used a rigid analytic model to represent the dark matter halo. Live dark matter halos could potentially introduce noise or allow secular instabilities to develop that could change our SFRs. To investigate this possibility we resimulate the IMMW created using the Springel (2000) initial conditions, but for these simulations we do not remove the dark matter. We use our fiducial concentrated blastwave feedback method and all the fiducial parameter values for the live halo simulations. We evolve all three resolutions: for the high resolution simulation we use one million dark matter particles to represent the dark halo and use the same relative number of particles for the other two resolutions. As we show in Figure 22, the addition of a live halo does not significantly change the mean SFRs at any resolution.

## 6.3 Summary of Chosen Parameters

Based on the constraints discussed in §6.1, we determined the parameter values in our star formation/supernova feedback recipe. We eliminated the Jeans Criterion used in Katz (1992) because it was sensitive to variations in resolution. Our parameter study using the  $\beta$  model converged towards the McKee & Ostriker (1977) analytic blastwave solution, so we chose to use the blastwave feedback method and concentrated the feedback to those particles that have their cooling

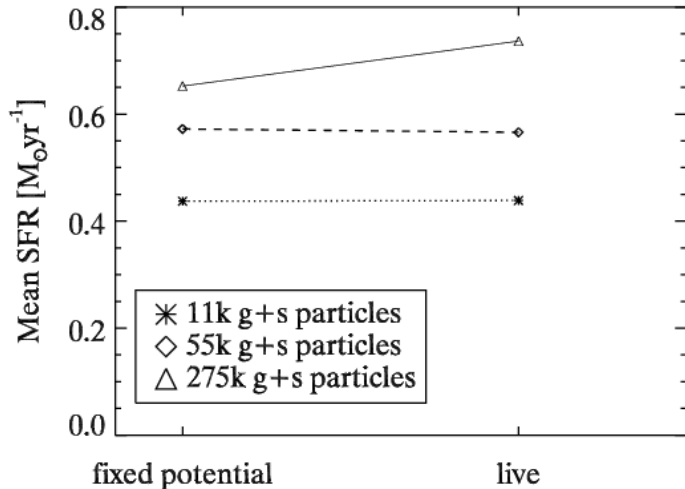


**Figure 22.** The mean SFR for the final blastwave model both with and without a live dark matter halo.

disabled. Employing this method means that there are only two free parameters,  $c^*$  and  $E_{\text{SN}}$ . We constrained the star formation efficiency,  $c^*$  to 0.05, which is close to the efficiency that Lada & Lada (2003) find in molecular clouds and star clusters. The mass of gas particles in the IMMW are close to the mass of molecular clouds, so this value for  $c^*$  seems reasonable. The amount of supernova energy transferred to the ISM,  $E_{\text{SN}}$ , is difficult to constrain using SFRs in a massive system like the IMMW since the galactic potential is so much deeper than the amount of energy that SN can inject into the ISM. The value of  $E_{\text{SN}} = 10^{50}$  ergs comes from comparing gas velocity dispersions and temperature distributions with observed values.

The blastwave model also requires that three criterion are met before stars can form:  $T_{\text{max}}$ ,  $n_{\text{min}}$  and that the gas is in an overdense virialised region. Gas particles may only form stars when their temperatures are below 15,000 K and is critical for making our SN feedback mechanism effective. Gas particles must also have a density above  $n_{\text{min}}=0.1 \text{ cm}^{-3}$ . The density criterion limits star formation to the dense regions of galaxies, which corresponds well to the density limits observed by Martin & Kennicutt (2001). The Katz (1992) argument that gas particles be part of a converging flow remains in our recipe because it does not have a major effect on the number of stars that form and might be useful in nonequilibrium situations.

#### 6.4 Comparison to Other Work

Several authors have recently proposed alternatives to the star formation recipe described in this paper. Both Kravtsov (2003) and Li et al. (2005a) have run simulations in which they do not impose a Schmidt Law for the star formation. Instead, they obtain this result naturally. While their studies shed considerable light on how stars form in the environment of a galaxy, our goal is to simply produce reasonable star formation rates in simulations and thus relies on the observations of Kennicutt (1998).

The Li et al. (2005a) recipe relies on high resolution simulations that at minimum satisfy the Bate & Burkert

(1997) resolution criteria. When simulations are run with an isothermal equation of state, the gas collapses because of instabilities into dense clumps where stars must form. Li et al. (2006) find that the collapse happens with the exact surface density dependence that Kennicutt (1998) observed. Kravtsov (2003) notices a steepening of the star formation rate with density in his simulations. The steepening led him to use a constant star formation timescale rather than a dynamical time that depends on density. Kravtsov (2003) argues that this type of behaviour is the result of a turbulent buildup of high density gas in such a way that the higher the density of the gas, the more high density, star forming gas is present. Kravtsov (2003) only uses thermal energy from supernovae as feedback, and hence it has little effect in his simulations. His need for altering the amount of star formation arises simply from how the gas collapses, and his adaptive mesh code may be more effective at resolving turbulence than our SPH code. However, the idea of changing the relationship between star formation and gas density could be useful for creating a recipe with realistic star formation at very high resolutions.

Tasker & Bryan (2006) run a set of simulations similar to Li et al. (2005b) except that they include supernova feedback and the gas is simulated on a grid. Even though their feedback implementation simply pours the feedback energy into the ISM, it proves effective at limiting star formation. The effectiveness of the feedback may be the result of high resolution, effective shock capture, and a more realistic cool curve using the Enzo AMR grid program. Even at the high resolutions, Tasker & Bryan (2006) find it necessary to use a recipe like Equation 4 that fixes the star formation dependence on density to a Schmidt law.

Recent observations also provide clues to a new physical recipe. Blitz & Rosolowsky (2004) base a recipe on molecular gas observations. The recipe is much like Elmegreen & Efremov (1997) in that it identifies gas pressure as the property most responsible for predicting SFRs. Observations also show interesting star formation behaviour in merging galaxies, the place where the most vigorous star formation happens in the local universe. Barnes (2004) has pointed out that current star formation recipes have a difficult time creating the starbursts observed in the shocked regions of merging galaxies, since star formation remains focused in the central regions of galaxies where the densities are high enough to facilitate star formation. It is yet to be seen whether or not our star formation formulation suffers from this problem.

## 7 CONCLUSIONS

Effective comparison of simulations with observations requires that simulations include gas and stars. Computational limitations prevent simulations from representing every atom or even every star in the universe. However, there are global properties of star formation (Kennicutt 1998) that can be reproduced in simulations. The simulations presented here use a scheme presented in Katz (1992) as a starting point. The maximum temperature, minimum density, converging flow, and stochastic selection of star forming gas particles from the Katz (1992) model were retained in our star formation recipe. However, the Jeans Criterion presented

in that work showed a strong resolution dependence in our simulations and was eliminated from our final star formation method.

Simulations of an isolated model Milky Way (IMMW) that only included this simple star formation recipe and pure thermal energy supernova feedback had SFRs that were higher than those observed. Therefore, we implemented an effective version of supernova feedback that uses the blast-wave solution presented in McKee & Ostriker (1977). Simulations cannot resolve the blastwave shocks from supernovae. Since star formation occurs in dense gas regions, when the supernova energy is simply distributed amongst nearby gas particles as thermal energy, it is quickly radiated away and produces no effective feedback. Thus, we chose to disable the radiative cooling of gas particles in the proximity of recently exploded supernovae so that the supernovae will suppress star formation. The Thacker & Couchman (2001) simulations showed the promise of this method, and we added the flexibility of how many gas particles have their cooling disabled to eliminate the resolution dependence of the Thacker & Couchman (2001) method.

After an initial attempt using a recipe containing many parameters (our  $\beta$  model), we settled on the treatment of supernova blastwaves presented in McKee & Ostriker (1977) to determine how many particles would have their cooling disabled. This proved an effective means for regulating star formation, and we were able to reproduce the Schmidt Law observed by Kennicutt (1998) with  $c^* = 0.05$ . Other than the feedback effect necessary to make the IMMW's star formation constant, the supernova feedback has little impact on star formation and we expect it to have little effect in other massive systems.

Our final star formation recipe is made up of these parameter values:

- $T_{\max}$  (maximum temperature) = 15,000 K
- must be in a virialised region
- $n_{\min}$  (minimum density) =  $0.1 \text{ cm}^{-3}$
- must be in a converging flow, i.e.  $\nabla \cdot \mathbf{v} < 0$
- $E_{\text{SN}}$  (energy transferred from SN to ISM) =  $10^{50}$  ergs
- $c^*$  (star formation efficiency) = 0.05
- $R_E$  (SN blast radius) =  $10^{1.74} E_{51}^{0.32} n_0^{-0.16} \tilde{P}_{04}^{-0.20} \text{ pc}$
- $t_{\max}$  (blast radius cooling time) =  $10^{6.85} E_{51}^{0.32} n_0^{0.34} \tilde{P}_{04}^{-0.70} \text{ yr}$

Given the success of our star formation method in the isolated Milky Way galaxy we hope it will continue in other situations. In future work we will investigate its performance when the galaxies have lower mass and see whether or not our feedback prescription can blow galactic winds like those observed. We are testing it on much more poorly resolved galaxies, like those that commonly arise in cosmological simulations. Finally, we are applying this method to cosmological simulations to see if we can reproduce the observed shallow faint end slope of the galaxy luminosity function.

## ACKNOWLEDGEMENTS

The anonymous referee made many detailed suggestions that greatly improved this paper. We are grateful to Volker Springel for his isolated galaxy model creation program. The authors wish to thank Julianne Dalcanton, Rob Thacker,

Octavio Valenzuela, Yuexing Li, T.J. Cox, Joel Primack, Naomi McClure-Griffiths and Mordecai Mac Low for useful conversations. Condor made managing all the simulations that we needed to run for this paper much easier. The Condor Software Program (Condor) was developed by the Condor Team at the Computer Sciences Department of the University of Wisconsin-Madison. All rights, title, and interest in Condor are owned by the Condor Team. The galaxy simulations were run on machines funded by the Student Technology Fee of the University of Washington. Large simulations were run on the supercomputers hosted at NCSA, ARSC, and University of Zurich. Many thanks to Joachim Stadel for allowing us to run some final, large simulations on zBox2. The analysis of the simulations presented in this paper used Salsa, funded by NASA ASIRP. Funding for this project was provided by NSF AST-0205969 and NASA NAGS-13308 & NNG04GK68G.

## REFERENCES

- Abel T., Anninos P., Zhang Y., Norman M. L., 1997, *New Astronomy*, 2, 181
- Alongi M., Bertelli G., Bressan A., Chiosi C., Fagotto F., Greggio L., Nasi E., 1993, *A&AS*, 97, 851
- Barnes J. E., 2004, *MNRAS*, 350, 798
- Bate M. R., Burkert A., 1997, *MNRAS*, 288, 1060
- Benz W., Thielemann F., 1990, *ApJ*, 348, L17
- Bertelli G., Bressan A., Chiosi C., Fagotto F., Nasi E., 1994, *A&AS*, 106, 275
- Black J. H., 1981, *MNRAS*, 197, 553
- Blitz L., Rosolowsky E., 2004, *ApJ*, 612, L29
- Bottama R., 2003, *MNRAS*, 344, 358
- Bressan A., Fagotto F., Bertelli G., Chiosi C., 1993, *A&AS*, 100, 647
- Broeils A. H., Rhee M.-H., 1997, *A&A*, 324, 877
- Brook C. B., Kawata D., Gibson B. K., Flynn C., 2004, *MNRAS*, 349, 52
- Burstein P., Borken R. J., Kraushaar W. L., Sanders W. T., 1977, *ApJ*, 213, 405
- Cen R., 1992, *ApJS*, 78, 341
- Cen R., Ostriker J. P., 1993, *ApJ*, 417, 415
- Chapman S. C., Blain A. W., Ivison R. J., Smail I. R., 2003, *Nature*, 422, 695
- Chevalier R. A., 1974, *ApJ*, 188, 501
- Colgate S. A., White R. H., 1966, *ApJ*, 143, 626
- Dickey J. M., Hanson M. M., Helou G., 1990, *ApJ*, 352, 522
- Dickey J. M., Lockman F. J., 1990, *ARAA*, 28, 215
- Elmegreen B. G., Efremov Y. N., 1997, *ApJ*, 480, 235
- Filippenko A. V., 1997, *ARAA*, 35, 309
- Gerritsen J. P. E., 1997, Ph.D. Thesis
- Gorenstein P., Harnden F. R., Tucker W. H., 1974, *ApJ*, 192, 661
- Governato F., Willman B., Mayer L., Brooks A., Stinson G., Valenzuela O., Wadsley J., Quinn T., 2006, *ArXiv Astrophysics e-prints* 0602351
- Hartmann L., 2002, *ApJ*, 578, 914
- Hernquist L., Katz N., 1989, *ApJS*, 70, 419
- Hultman J., Pharasyn A., 1999, *A&A*, 347, 769
- Jenkins E. B., Meloy D. A., 1974, *ApJ*, 193, L121

- Jones K. L., Koribalski B. S., Elmouttie M., Haynes R. F., 1999, *MNRAS*, 302, 649
- Katz N., 1992, *ApJ*, 391, 502
- Katz N., Weinberg D. H., Hernquist L., 1996, *ApJS*, 105, 19
- Kawata D., Gibson B. K., 2003, *MNRAS*, 340, 908
- Kennicutt R. C., 1998, *ApJ*, 498, 541
- Kennicutt R. C., Tamblyn P., Congdon C. E., 1994, *ApJ*, 435, 22
- Kim S., Staveley-Smith L., Dopita M. A., Sault R. J., Freeman K. C., Lee Y., Chu Y., 2003, *ApJS*, 148, 473
- Klypin A., Zhao H., Somerville R. S., 2002, *ApJ*, 573, 597
- Kravtsov A. V., 1999, Ph.D. Thesis
- Kravtsov A. V., 2003, *ApJ*, 590, L1
- Lada C. J., Lada E. A., 2003, *ARAA*, 41, 57
- Larson R. B., 1969, *MNRAS*, 145, 405
- Li Y., Mac Low M.-M., Klessen R. S., 2005a, *ApJ*, 620, L19
- Li Y., Mac Low M.-M., Klessen R. S., 2005b, *ApJ*, 626, 823
- Li Y., Mac Low M.-M., Klessen R. S., 2006, *ApJ*, 639, 879
- Lia C., Portinari L., Carraro G., 2002, *MNRAS*, 330, 821
- Marri S., White S. D. M., 2003, *MNRAS*, 345, 561
- Martin C. L., Kennicutt R. C., 2001, *ApJ*, 555, 301
- McKee C. F., Ostriker J. P., 1977, *ApJ*, 218, 148
- Michel-Dansac L., Wozniak H., 2004, *A&A*, 421, 863
- Miller G. E., Scalo J. M., 1979, *ApJS*, 41, 513
- Monaghan J. J., 1992, *ARAA*, 30, 543
- Navarro J. F., Frenk C. S., White S. D. M., 1997, *ApJ*, 490, 493
- Navarro J. F., White S. D. M., 1993, *MNRAS*, 265, 271
- Okamoto T., Eke V. R., Frenk C. S., Jenkins A., 2005, *MNRAS*, 363, 1299
- Okamoto T., Jenkins A., Eke V. R., Quilis V., Frenk C. S., 2003, *MNRAS*, 345, 429
- O’Shea B. W., Bryan G., Bordner J., Norman M. L., Abel T., Harkness R., Kritsuk A., 2004, *Adaptive Mesh Refinement - Theory and Applications*
- Padmanabhan T., 2001, *Theoretical Astrophysics, Volume 2: Stars and Stellar Systems. Theoretical Astrophysics, Volume 2: Stars and Stellar Systems*, by T. Padmanabhan. Cambridge University Press, 2001, 594 pp.
- Pearce F. R., Jenkins A., Frenk C. S., Colberg J. M., White S. D. M., Thomas P. A., Couchman H. M. P., Peacock J. A., Efstathiou G., *The Virgo Consortium 1999*, *ApJ*, 521, L99
- Pelupessy F. I., van der Werf P. P., Icke V., 2004, *A&A*, 422, 55
- Raiteri C. M., Villata M., Navarro J. F., 1996, *A&A*, 315, 105
- Reid I. N., Gizis J. E., Hawley S. L., 2002, *AJ*, 124, 2721
- Rocha-Pinto H. J., Maciel W. J., 1997, *MNRAS*, 289, 882
- Scannapieco C., Tissera P. B., White S. D. M., Springel V., 2005, *MNRAS*, 364, 552
- Schmidt M., 1959, *ApJ*, 129, 243
- Silk J., 1987, in *IAU Symp. 115: Star Forming Regions Star formation and galactic evolution - From protogalaxies to starbursts*. pp 663–689
- Silk J., 2003, *MNRAS*, 343, 249
- Sommer-Larsen J., Götz M., Portinari L., 2003, *ApJ*, 596, 47
- Springel V., 2000, *MNRAS*, 312, 859
- Springel V., Hernquist L., 2002, *MNRAS*, 333, 649
- Springel V., Hernquist L., 2003, *MNRAS*, 339, 289
- Tasker E. J., Bryan G. L., 2006, *ApJ*, 639, 879
- Telesco C. M., 1988, *ARAA*, 26, 343
- Thacker R. J., Couchman H. M. P., 2000, *ApJ*, 545, 728
- Thacker R. J., Couchman H. M. P., 2001, *ApJ*, 555, L17
- Thielemann F.-K., Nomoto K., Yokoi K., 1986, *A&A*, 158, 17
- Thornton K., Gaudlitz M., Janka H.-T., Steinmetz M., 1998, *ApJ*, 500, 95
- van den Bergh S., McClure R. D., 1994, *ApJ*, 425, 205
- van der Hulst J. M., 1996, in *ASP Conf. Ser. 106: The Minnesota Lectures on Extragalactic Neutral Hydrogen Bubbles and Holes in the Interstellar Medium*. pp 47–+
- Verner D. A., Ferland G. J., 1996, *ApJS*, 103, 467
- Wadsley J. W., Stadel J., Quinn T., 2004, *New Astronomy*, 9, 137
- Weidemann V., 1987, *A&A*, 188, 74
- Wong T., Blitz L., 2002, *ApJ*, 569, 157
- Woosley S. E., Weaver T. A., 1995, *ApJS*, 101, 181
- Yepes G., Kates R., Khokhlov A., Klypin A., 1997, *MNRAS*, 284, 235
- York D. G., 1974, *ApJ*, 193, L127